The Abdus Salam International Centre for Theoretical Physics

United Nations Educational, Scientific and Cultural Organization

IAEA International Atomic Energy Agency

2137-28

Joint ICTP-IAEA Advanced Workshop on Multi-Scale Modelling for Characterization and Basic Understanding of Radiation Damage Mechanisms in Materials

12 - 23 April 2010

Molecular dynamics simulation of primary damage formation and phase transformations in zirconium

N. Lazarev

Akhiezer Institute for Theoretical Physics
Kharkov
Ukraine

Molecular dynamics simulation of primary damage formation and phase transformations in zirconium

Nikolai Lazarev

Kharkov Institute of Physics and Technology, Ukraine

n.lazarev@kipt.kharkov.ua

Collaboration:

Alexander S. Bakai
Tatyana P. Chernyaeva
Anatole A. Turkin
Kharkov Institute of Physics and Technology, Ukraine

Graeme J. Ackland
University of Edinburgh, Scotland, UK

Motivation

Zirconium based alloys are a widely investigated materials due to applications in nuclear reactors and peculiar properties at phase transformations and plastic deformations

Two main alloys: Zircaloy and Zr-2.5Nb are poor neutron adsorber and are used as a nuclear fuel can material and for CANDU pressure tubes

Creep resistance of Zr-2.5Nb is good up to ~330 C

Creep ductility of Zircaloy is high: use as fuel can

The main problem is *radiation growth*

Mechanisms of c-loops nucleation?

Martensitic transformation

Outline

Diffusion of point defects

Martensitic Phase Transformation in Zr

Hysteretic behavior at reversible MT

Thermodynamics of MT and temperature T_0

Local structural order (LSO) parameter

Kinetics of transformation

Heterogeneous nucleation on free surface

MT in polycrystalline Zr

Primary damages in displacement cascades

Conclusions

Most important Bravais lattices of simple metals

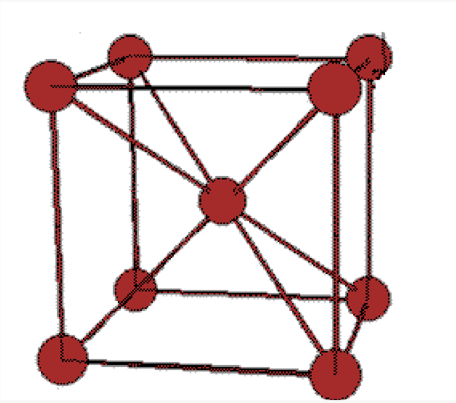

bcc

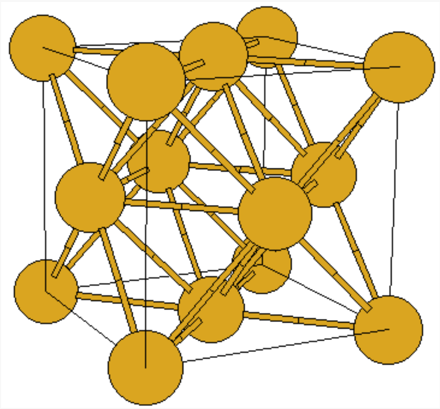

fcc

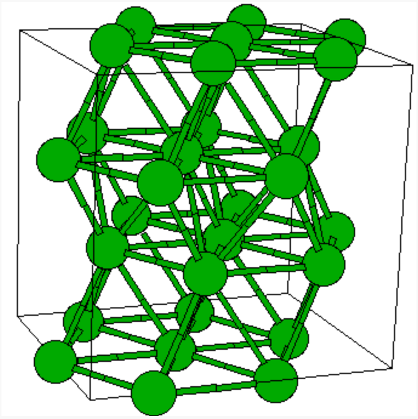

hcp

Simple metal lattice types

H																	He
453.69 Li bcc	1560 Be hcp											B	C	N	O	F	Ne
370.87 Na bcc	923 Mg hcp											933.47 Al fcc	Si	P	S	Cl	Ar
336.53 K bcc	1115 Ca fcc	1814 Sc hcp	1941 Ti hcp	2183 V bcc	2180 Cr bcc	1519 Mn	1811 Fe bcc	1768 Co hcp	1728 Ni fcc	1357.8 Cu fcc	692.68 Zn	301.91 Ga	Ge	As	Se	Br	Kr
312.46 Rb bcc	1050 Sr fcc	1799 Y hcp	2128 Zr hcp	2750 Nb bcc	2896 Mo bcc	2430 Tc hcp	2607 Ru hcp	2237 Rh fcc	1828 Pd fcc	1235 Ag fcc	594 Cd	430 In	505 Sn	904 Sb	Te	I	Xe
302 Cs bcc	1000 Ba bcc		2506 Hf hcp	3290 Ta bcc	3422 W bcc	3186 Re hcp	3033 Os hcp	2446 Ir fcc	1768 Pt fcc	1337.33 Au fcc	234.32 Hg	577 Tl hcp	600.61 Pb fcc	544.7 Bi	Po	At	Rn
Fr	Ra bcc		Rf	Db	Sg	Bh	Hs	Mt	Ds	Rg	Uub	Uut	Uuq	Uup	Uuh	Uus	Uuo
		↓															
		La	Ce fcc	Pr	Nd	Pm hcp	Sm	Eu bcc	Gd hcp	Tb hcp	Dy hcp	Ho hcp	Er hcp	Tm hcp	Yb fcc	Lu hcp	
		Ac fcc	Th fcc	Pa	U	Np	Pu	Am hcp	Cm hcp	Bk	Cf	Es	Fm	Md	No	Lr	

Directions in HCP crystals

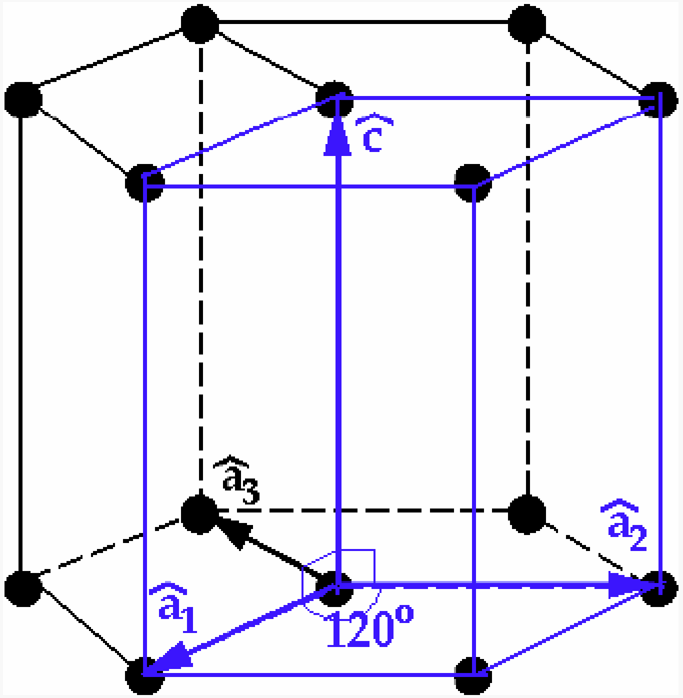

4-coordinate system is used:

$$[\hat{a}_1, \hat{a}_2, \hat{a}_3, c]$$

$$\hat{a}_3 = -(\hat{a}_1 + \hat{a}_2)$$

Indexes of some planes and directions in HCP lattice

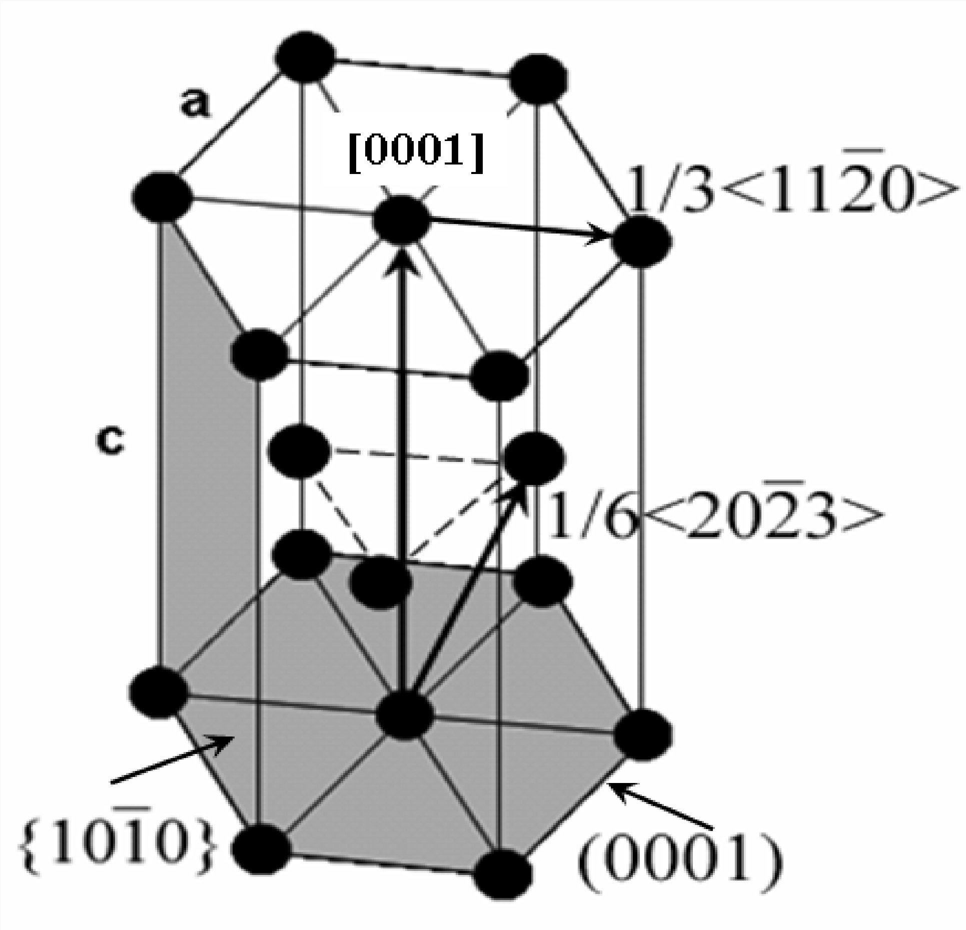

Dislocation loops in HCP crystals nucleated on prismatic {1010}, basal (0001) and pyramidal {1011} planes have Burgers vectors (1/3)<1120>, (1/6)<2023> or (1/2)[0001] and (1/3)<1123> respectively.

Oxygen influence on <c> loop nucleation

O.V. Borodin et al, Problems of Atomic Sc. Tech. (2008)

Zr^{6+}, 15 dpa, T=550^{o}C

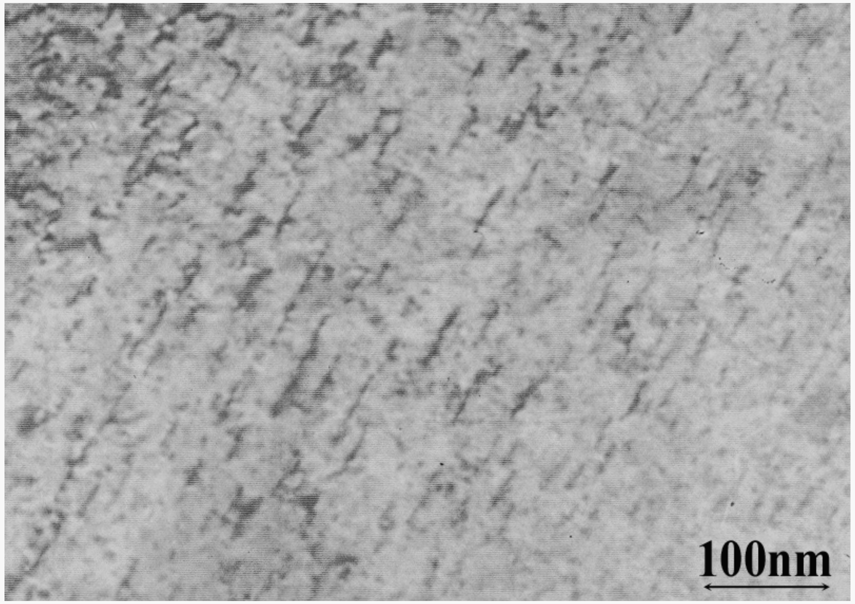

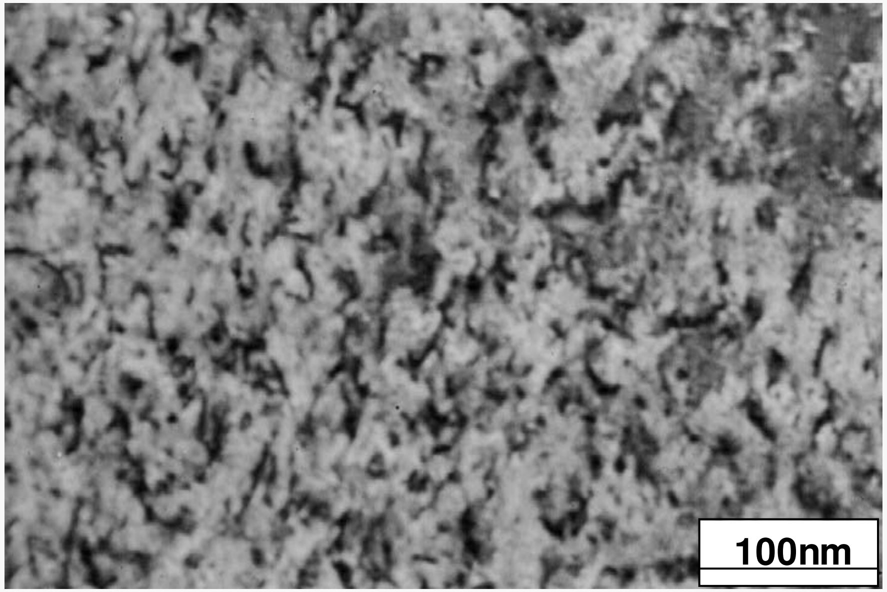

Zr-1%Nb + 0,08% O_2

Zr-1%Nb + 0,19% O_2

The formation of <c>-loops is observed at low O_2 content. Increasing of oxygen concentration up to 0,19% completely suppress their nucleation.

Simulation Setup

Molecular Dynamics with Empirical force-field

EAM potential: $U = \sum_{ij} V(r_{ij}) + \sum_{i} F(\bar{\rho}_i)$, $\bar{\rho}_i = \sum_{j} \phi(r_{ij})$

Parameterization:

M.I. Mendelev, G.J. Ackland, Phil. Mag. Lett. 87 (2007) p. 349. (MA)

M. Igarashi, M. Khantha, V. Vitek, Phil. Mag. B63 (1991) 603. (IKV).

G.J. Ackland, S.J. Wooding, D.J. Bacon, Phil. Mag. A 71 (1995) 553 (AWB).

R.C. Pasianot, A.M. Monti, J. Nuclear Materials 264 (1999) 198. (PM)

Physical properties calculated for various interatomic potentials

Property	Target value	AWB	PM	IKV	#1	#2	#3
a (hcp) (Å)	3.232[1]	3.249	3.232	3.232	3.231	3.220	3.234
c (hcp) (Å)	5.182[1]	5.183	5.149	5.149	5.186	5.215	5.168
E_{coh} (eV/atom)	-6.32[2]	-6.250	-6.250	-6.250	-6.017	-6.469	-6.635
C_{11} (hcp, GPa)	155[3]	160	146	155	196	165	147
C_{12} (hcp, GPa)	67[3]	76	70	67	88	65	69
C_{44} (hcp, GPa)	36[3]	36	32	36	47	48	44
C_{13} (hcp, GPa)	65[3]	70	65	65	81	63	74
C_{33} (hcp, GPa)	172[3]	174.7	164.8	173	212	180	168
E_f^V (unrelaxed) (hcp, eV)	2.077[4]	1.817	1.780	1.830	1.550	2.310	1.762
Octahedral interstitial (T=0)	2.84[5]	4.13	2.81	8.01	3.23	3.51	2.88
Basal octahedral interstitial (T=0)	2.88[5]	3.98	2.63	9.10	3.02	2.87	2.90
Basal crowdion interstitial (T=0)	2.95[5]	3.82	2.56	8.50	3.25	3.35	2.91
I_2 basal stacking fault defect energy (meV/Å^2)	12.5[9]	3.3	4.4	1.7	6.3	6.8	12.4
Prism stacking fault defect energy (meV/Å^2)	9.1[9]	unstable	10.1	unstable	unstable	23.3	10.9
a (fcc) (Å)	4.53[4]	4.571	4.543	4.553	4.557	4.545	4.538
$\Delta E_{hcp\to fcc}$ (eV/atom)	0.032[4]	0.013	0.018	0.007	0.028	0.030	0.054
a (bcc) (Å)	3.57[4]	3.589	3.568	3.644	3.592	3.562	3.576
$\Delta E_{hcp\to bcc}$ (eV/atom)	0.071[4]	0.030	0.053	0.111	0.024	0.052	0.103
C_{11} (bcc, GPa)	82[4]	119	111	56	114	96	50
C_{12} (bcc, GPa)	93[4]	119	117	118	98	109	94
C_{44} (bcc, GPa)	29[4]	83	60	113	63	42	50
$T_{\alpha\to\beta}$ (K)	1136[6]	2054 > T_m	1211 >T_m	1251	588	1233	1385
$\Delta H_{\alpha\to\beta}$ (eV/atom)	0.040[6]	0.054	0.041	0.037	0.019	0.039	0.058
$\Delta V_{\alpha\to\beta}/V_\alpha$ (%)	-0.4[7]	+1.3	+1.9	+4.9	-1.5	-0.8	+0.9
T_m (hcp, K)		1778	1045	1765	1555	1913	1369
T_m (bcc, K)	2128[6]	1681	950	1887	1692	2109	1358
T_m (fcc, K)		1750	988	1739	unstable	unstable	unstable
d (liquid, T=2128 K) (atom/nm^3)	39.56[8]	37.19	37.26	31.39	38.55	40.08	39.65
ΔH_m (eV/atom)	0.151[6]	0.161	0.108	0.103	0.167	0.179	0.078
$\Delta V_m/V_s$ (%)	3.9[6]	4.5	3.7	3.4	4.9	2.6	1.2

Temperature dependence of axial ratio *c/a*

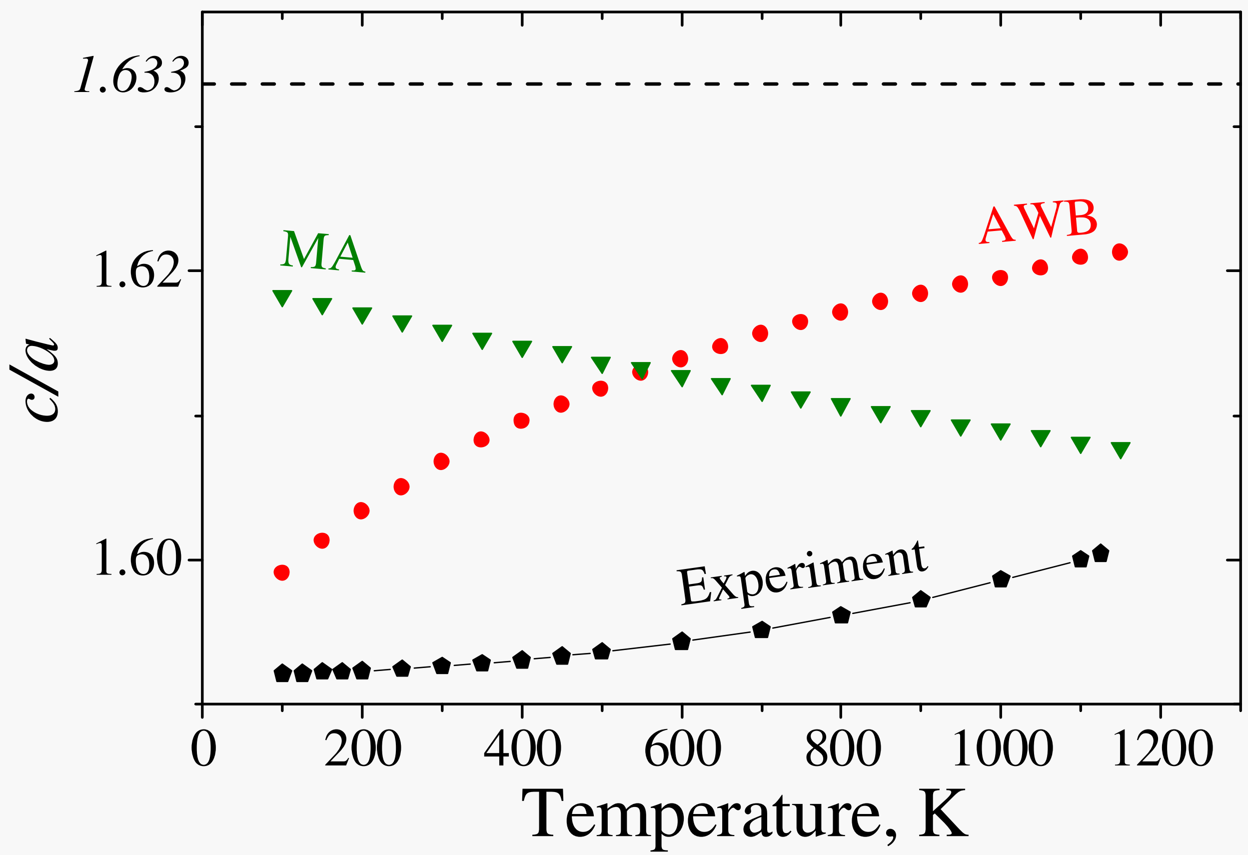

Diffusion of point defects

MA

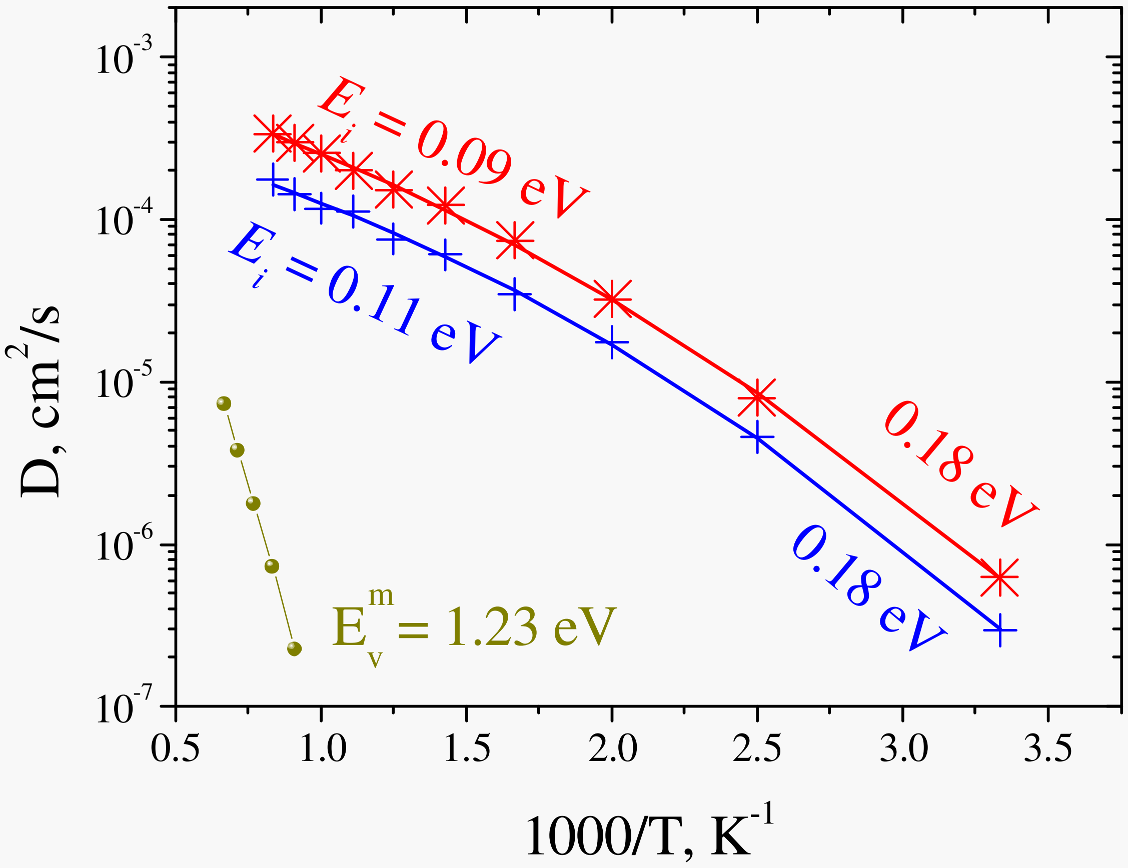

AWB

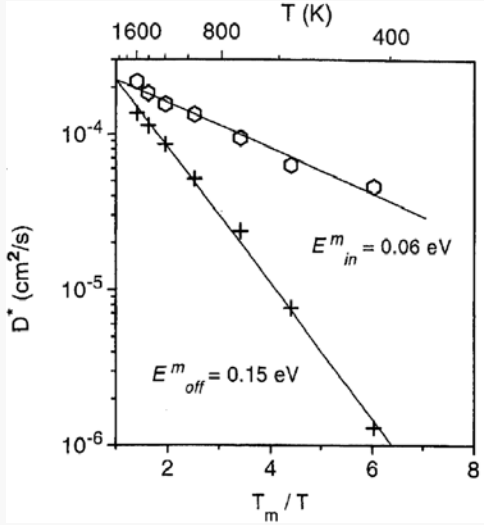

Possible configurations of SIA in HCP lattice

C.H. Woo, Hanchen Huang and W.J. Zhu, Appl. Phys. A76 (2003) 101

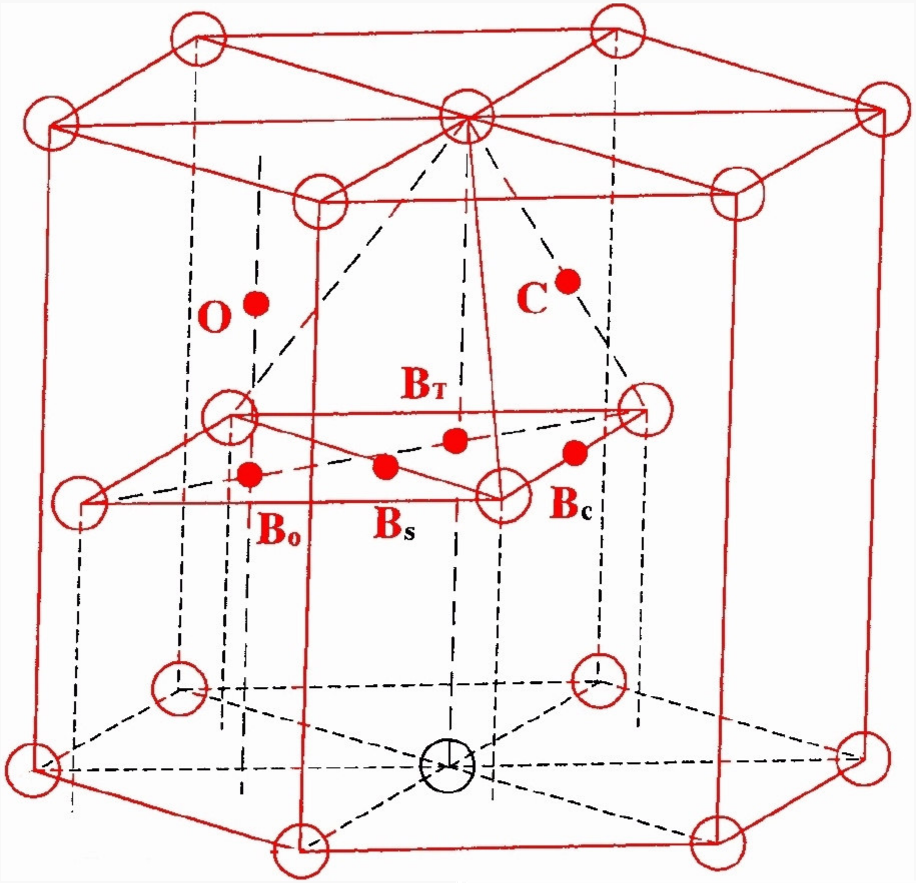

Octahedral (**O**)

Basal tetrahedral (**B_T**)

Basal octahedral (**B_O**)

Basal crowdion (**B_C**)

Basal split (**B_S**)

Non-basal crowdion (**C**)

c-dumbbell (**D_C**)

Configuration	B_C	B_S	B_O	B_T	O	C
Ackland (eV)	3.71	3.72	3.93	3.98	4.08	3.93
Pasianot (eV)	3.75	3.76	3.88	4.05	4.05	4.03
	Stable	Unstable	Metastable	Unstable	Unstable	Unstable

Point defect diffusivities

a) Via calculation of atomic displacements

$$D_a = f_d C_d D_d \qquad f_v = \begin{cases} 0.653, & \text{sc} \\ 0.782, & fcc \end{cases}$$

$$D_d = D_a / f_d C_d$$

$$D_a = < \Delta r^2 > / 6t$$

b) Direct tracing of defect diffusion

$$t_j = \Delta t \cdot j \qquad R^2 = \sum_j (r_j - r_{j-1})^2$$

$$D \rightarrow R^2 / 6N\Delta t$$

$$D_c = < (z_j - z_{j-1})^2 > / 2\Delta t$$

Why f_i can be very small?

1-*a* space jumps: dumbbell SIA motion

After k jumps mean-squared displacement

of SIA $r_{\text{int}}^2 \rightarrow k \cdot a^2$

and atoms $r_{atoms}^2 \rightarrow k \cdot a^2$ $D_{atoms} \rightarrow C_{\text{int}} D_{\text{int}}$

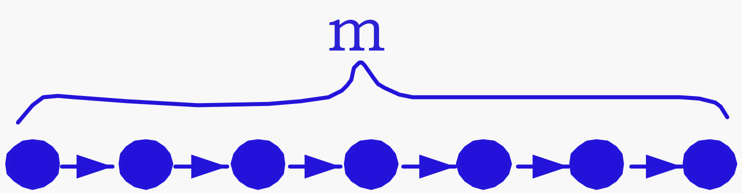

m-a **space jumps:** crowdion motion

$$r_{\text{int}}^2 \rightarrow k \cdot (ma)^2$$

$$r_{atoms}^2 \rightarrow k \cdot ma^2 \qquad D_{atoms} \rightarrow \frac{1}{m} C_{\text{int}} D_{\text{int}}$$

Crowdion motion of SIA

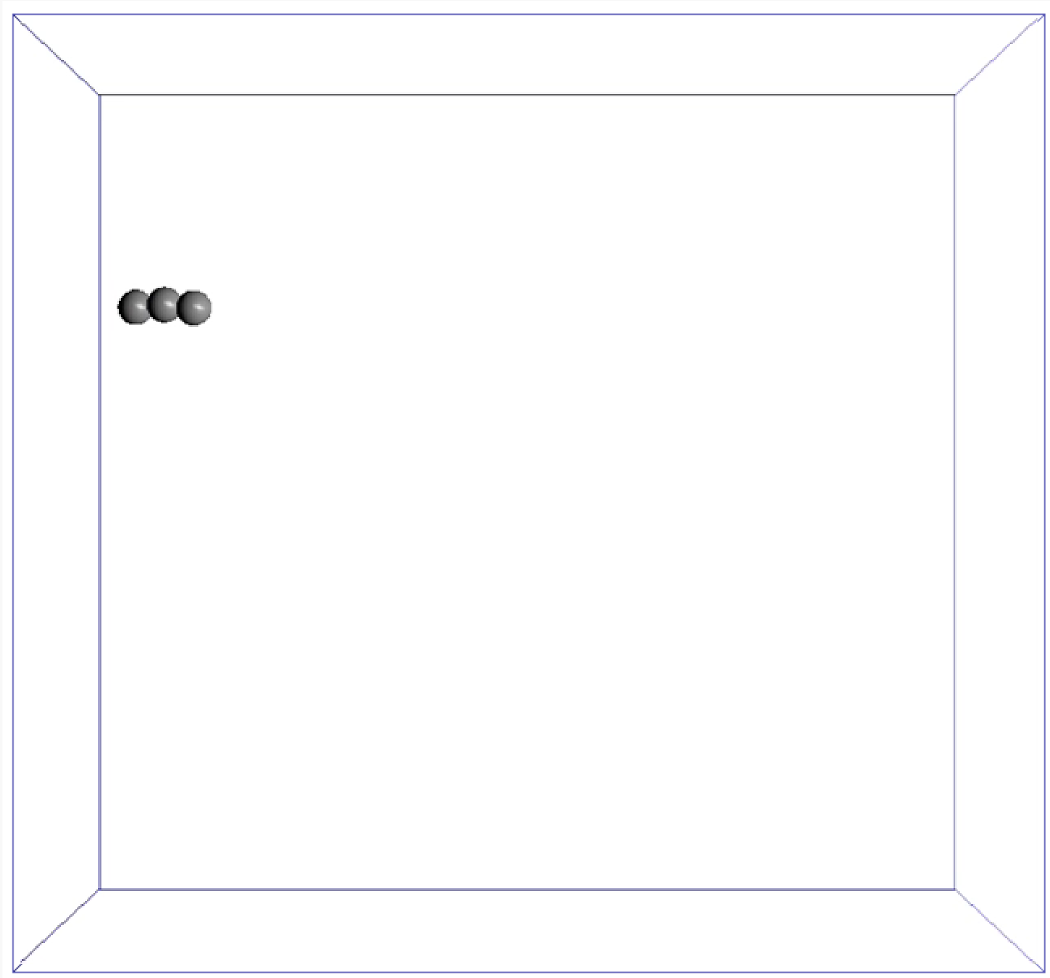

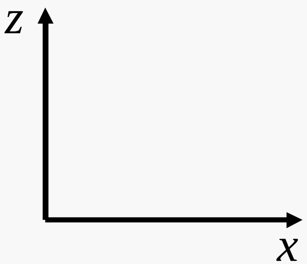

movie

Crowdion motion of SIA

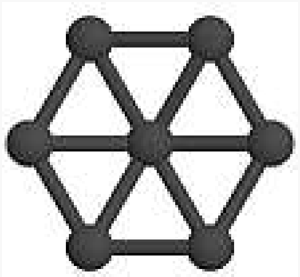

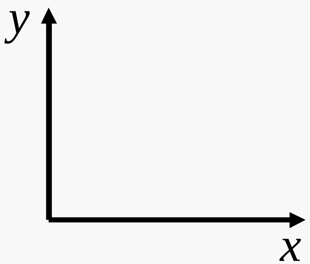

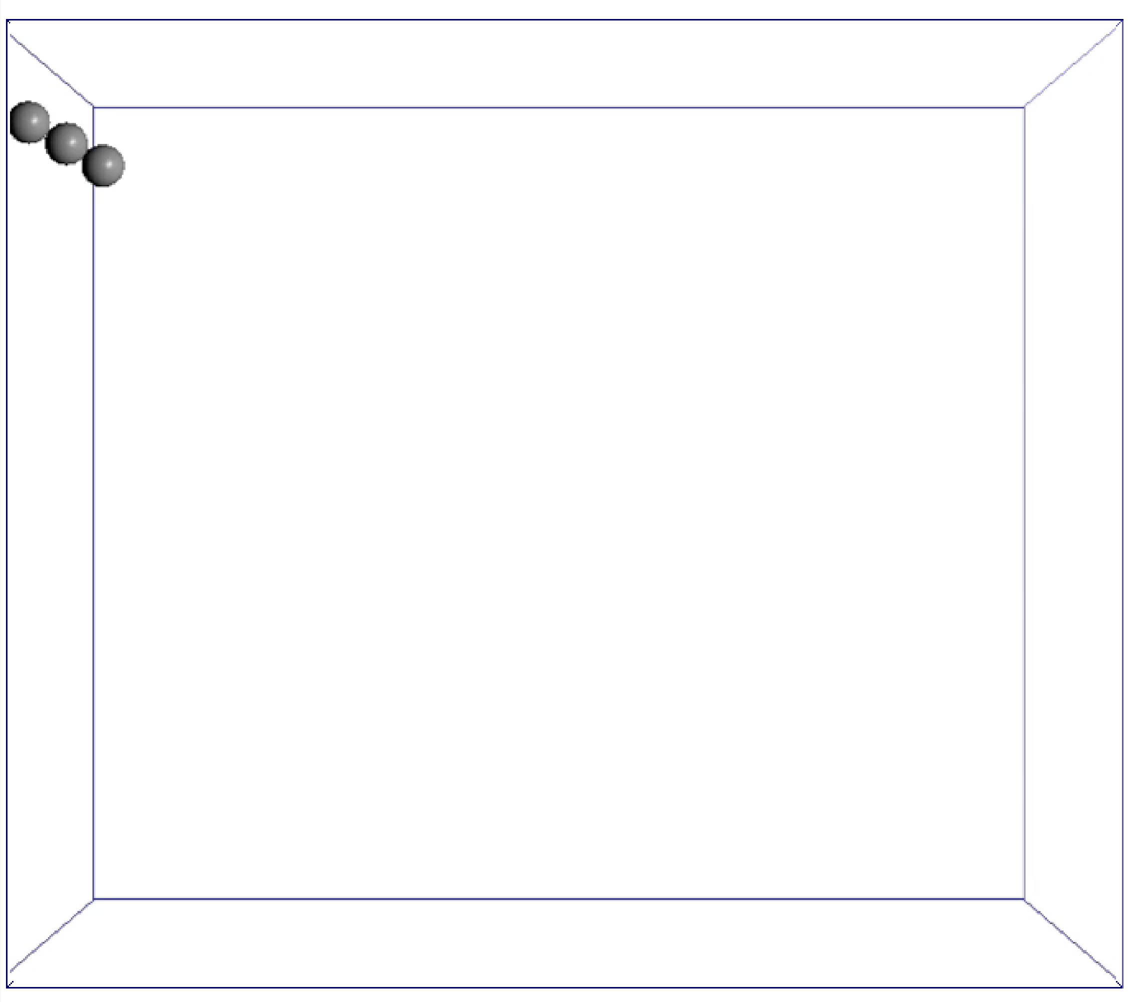

movie

Interstitial self-diffusion?

Phase	Defect	E_f at T=1000 K	E_m	E_f+E_m	E_D (experiment)
hcp	Vacancy	2.38	1.23	3.61	3.17
	Interstitial	3.17	0.11	3.28	
bcc	Vacancy	2.00	0.44	2.44	2.04
	Interstitial	2.04	0.11	2.15	

Martensitic Phase Transformation in Zr

α-Zr $\rightarrow$ β-Zr at T = 1136 K

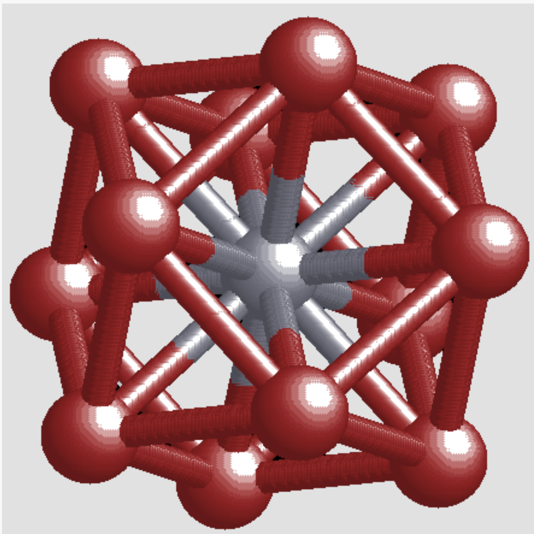

HCP

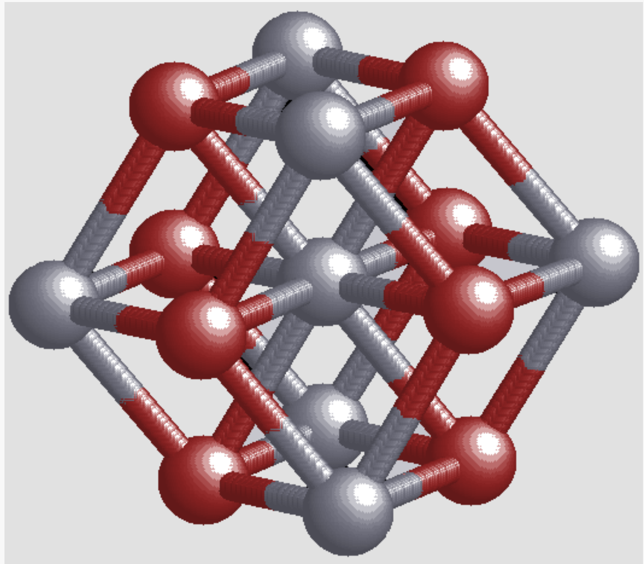

BCC

“Kinetic Phase Diagram”

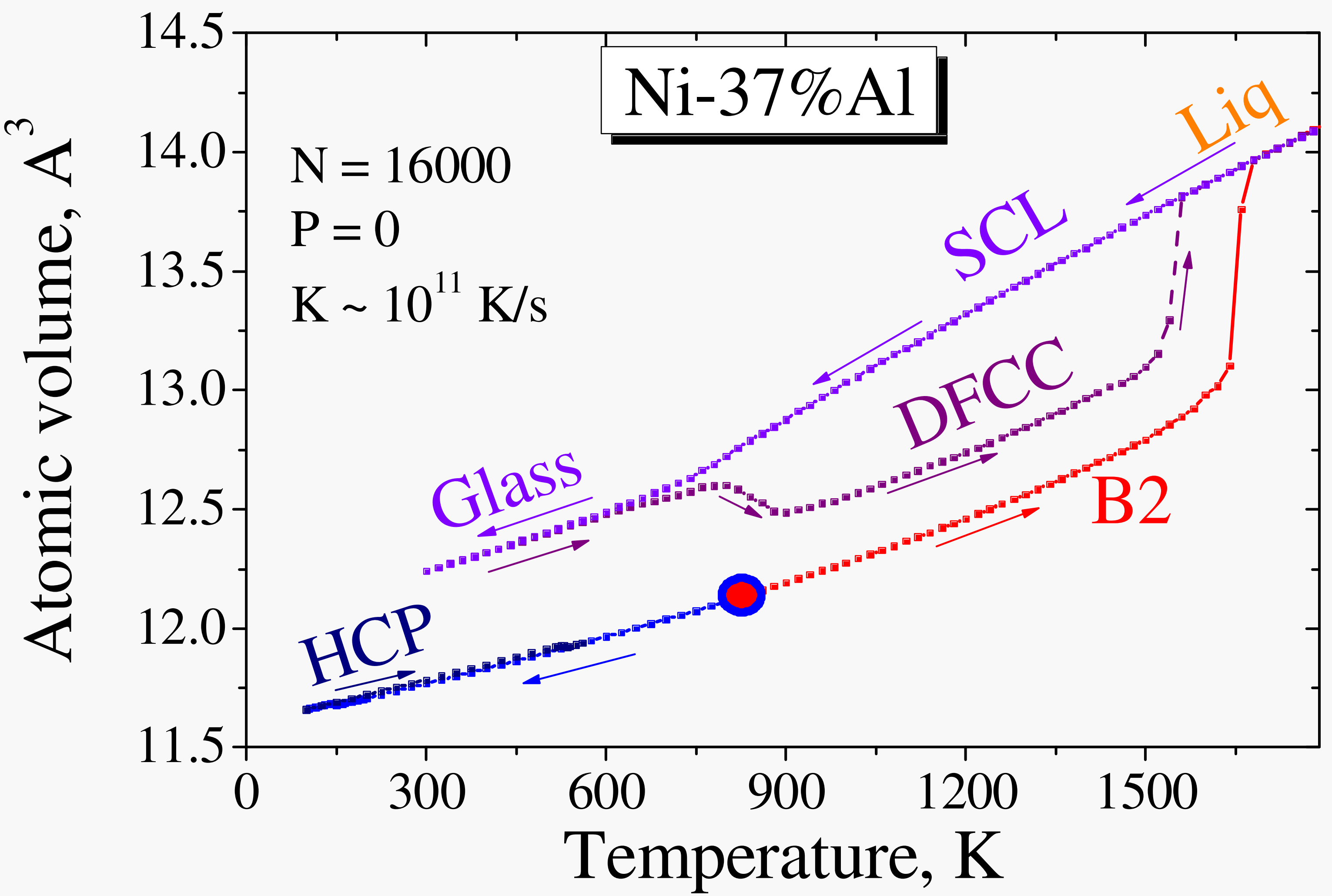

Enthalpy at Reversible Temperature-Controlled MT

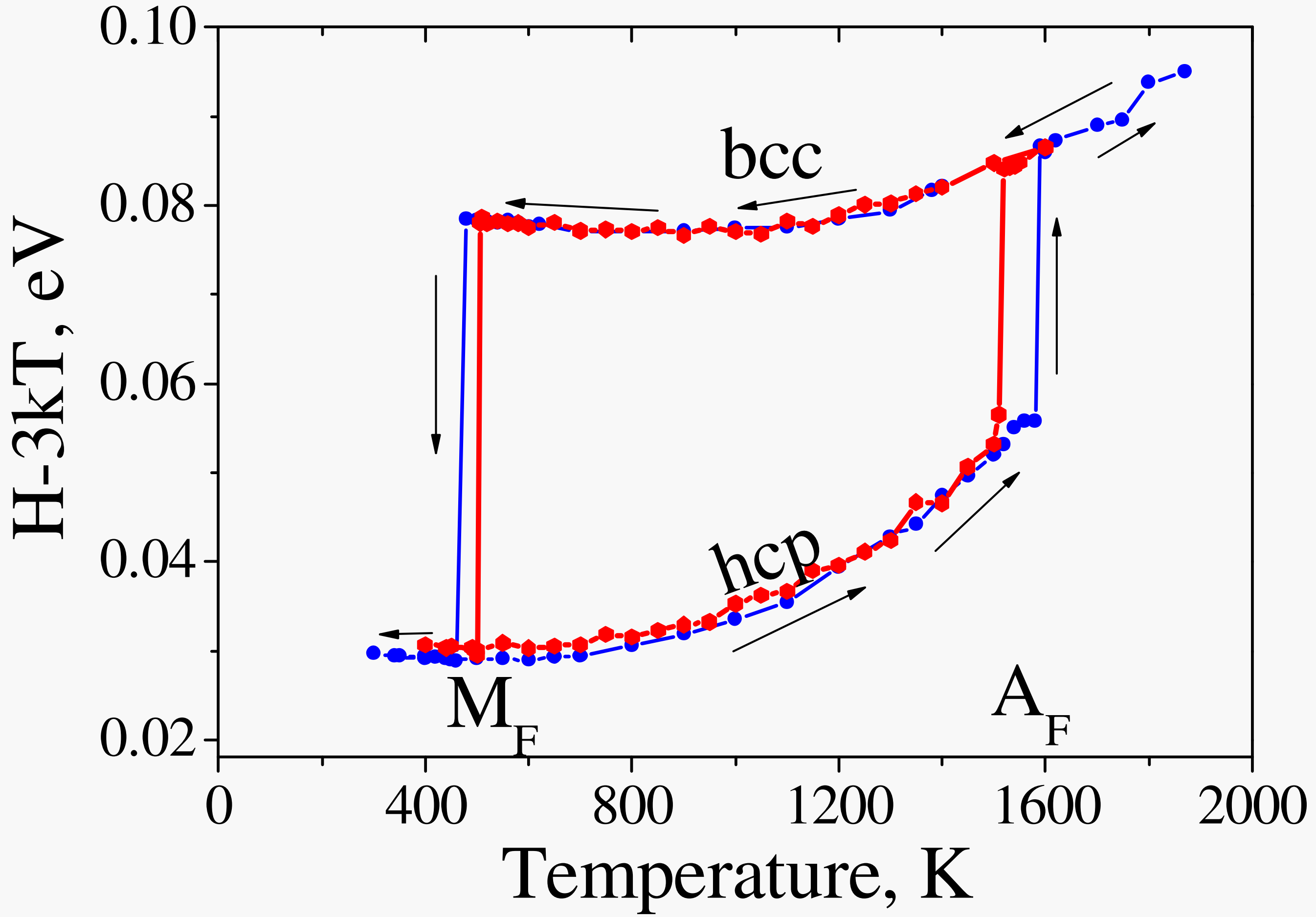

- *The 1-st order phase transformations:* $A \to M \to A$

Thermodynamics of MT and temperature T_0

$$F = H - TS$$

$$S = -\left.\frac{\partial F}{\partial T}\right|_{P=0} \qquad \frac{d}{dT}\left(\frac{F}{T}\right) = -\frac{H}{T^2}$$

$$\frac{\Delta F(T)}{T} = \frac{\Delta F(T_1)}{T_1} - \int_{T_1}^{T} \left[\Delta H(\tau)/\tau^2\right] d\tau$$

$$\Delta S_{AM} = ?$$

Entropy of harmonic system

$$S_{har} = -k_B \sum_j \ln(\hbar\omega_j / k_B T) + S_0$$

$$\Delta S_{AM} = -\int_0^\infty \ln(\omega)[g_A(\omega) - g_M(\omega)]d\omega = -\ln\frac{\overline{\omega}_A}{\overline{\omega}_M}$$

$$A_{VV}(t) = \int_0^\infty V(\tau)V(\tau + t)d\tau$$

$$g(\omega) = \frac{1}{2\pi}\int_0^\infty e^{-\omega t} A_{VV}(t)dt$$

Spectral densities in martensite and austenite phases

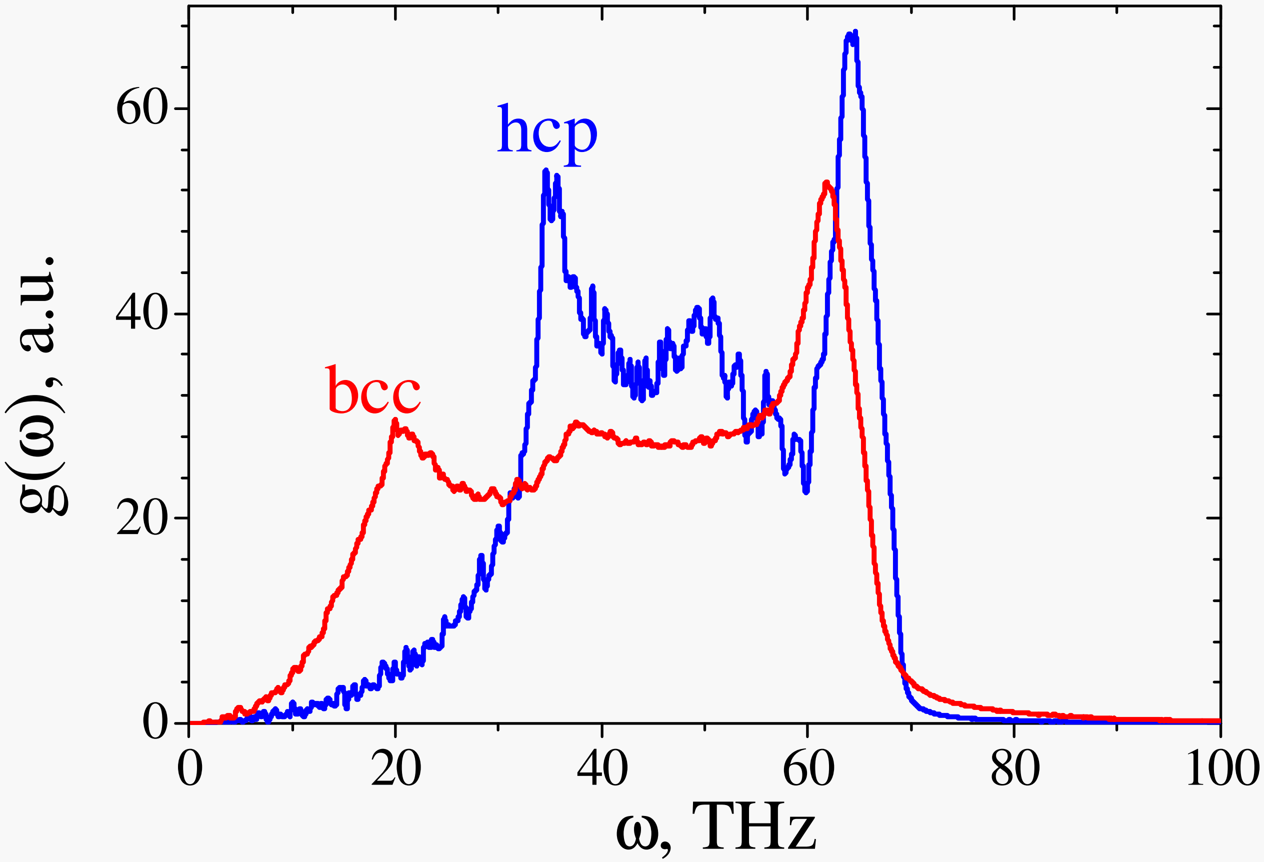

- $\Delta S_{\alpha\beta} = 0.45k$

Free energy difference

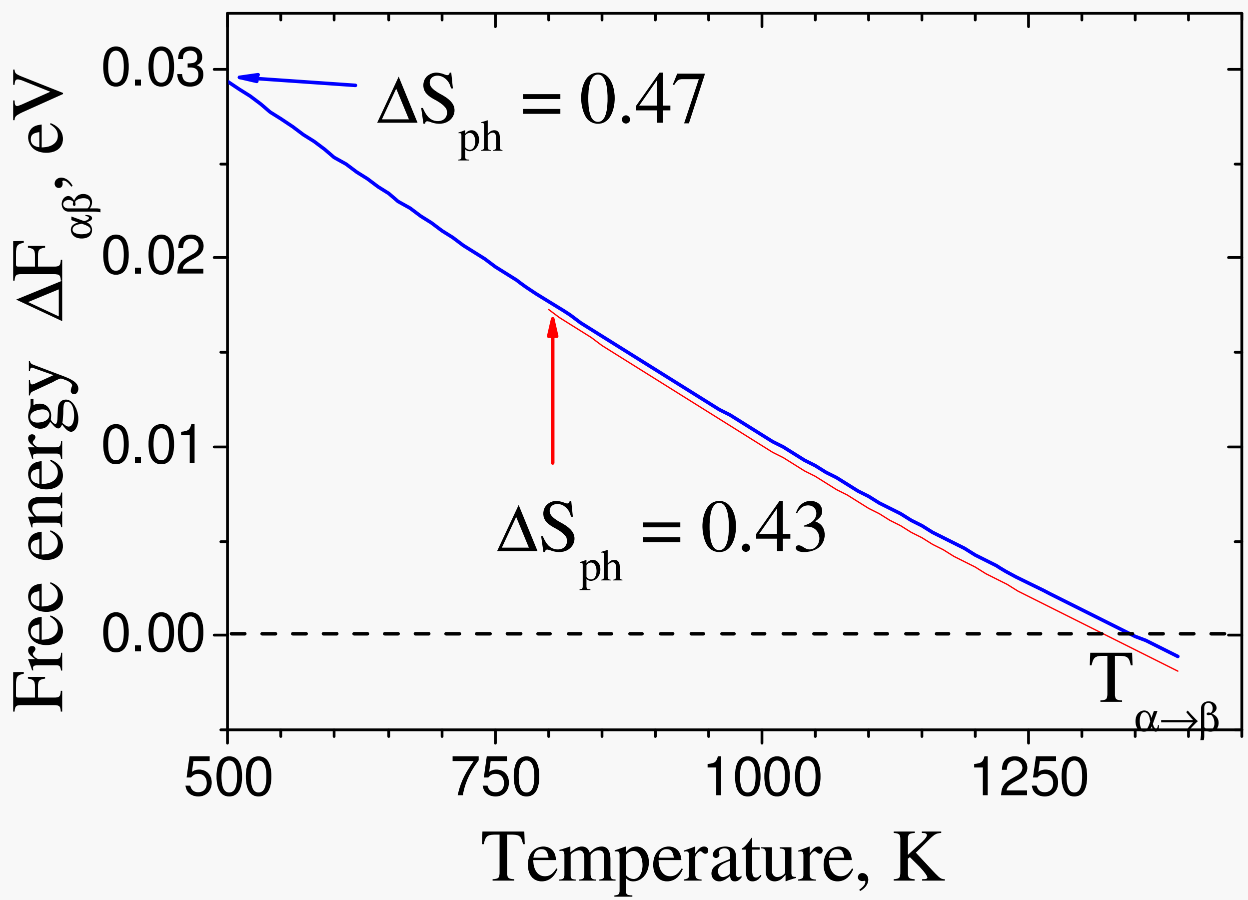

- $T_0 \approx 1340\ K$

Phase coexistence, T_c

Ni_7Al_5

T = 450K, N = 1809648

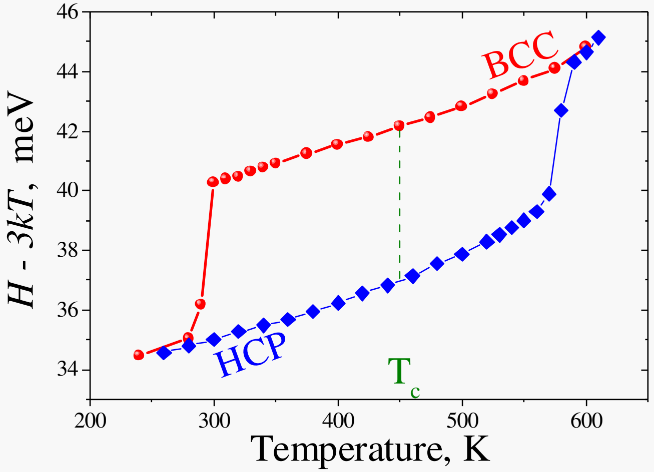

Perfect FCC+HCP

Distorted FCC+HCP

Perfect BCC

Distorted BCC

Perf. & Dist. ICO

Unclassified

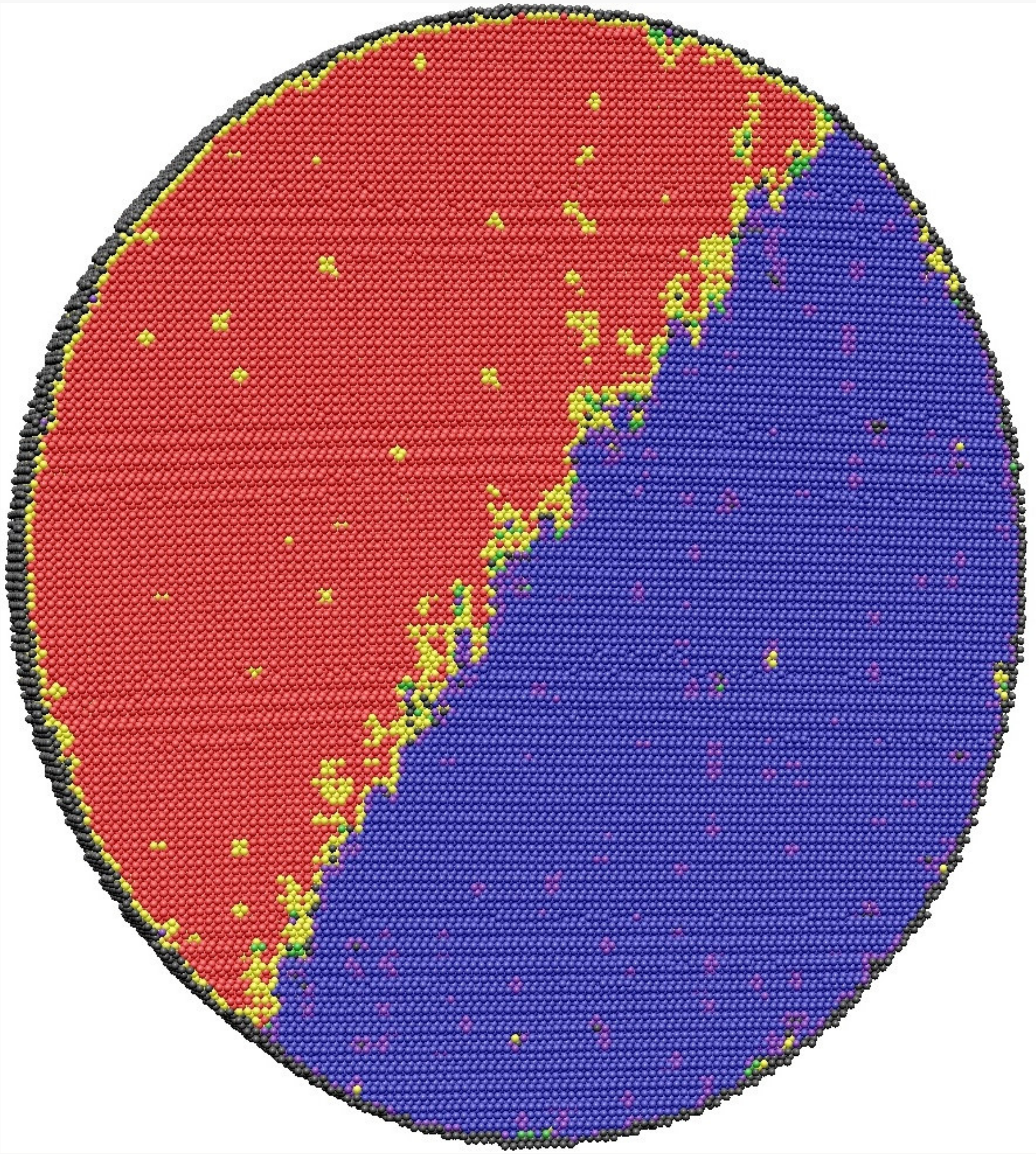

Phase coexistence, T_c

Ni_7Al_5
T = 450K, N = 1809648

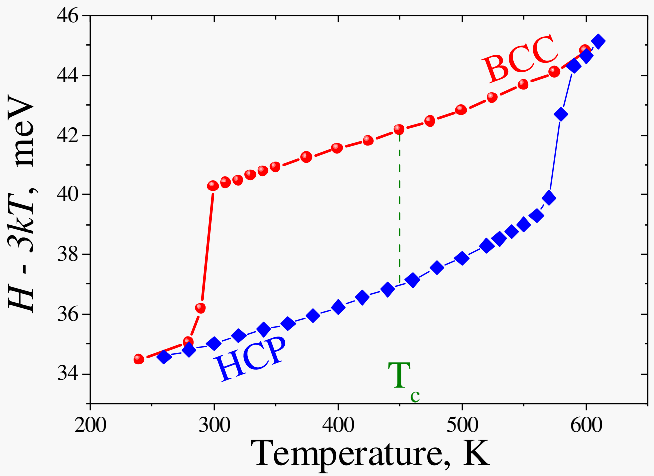

Perfect FCC+HCP
Distorted FCC+HCP
Perfect BCC
Distorted BCC
Perf. & Dist. ICO
Unclassified

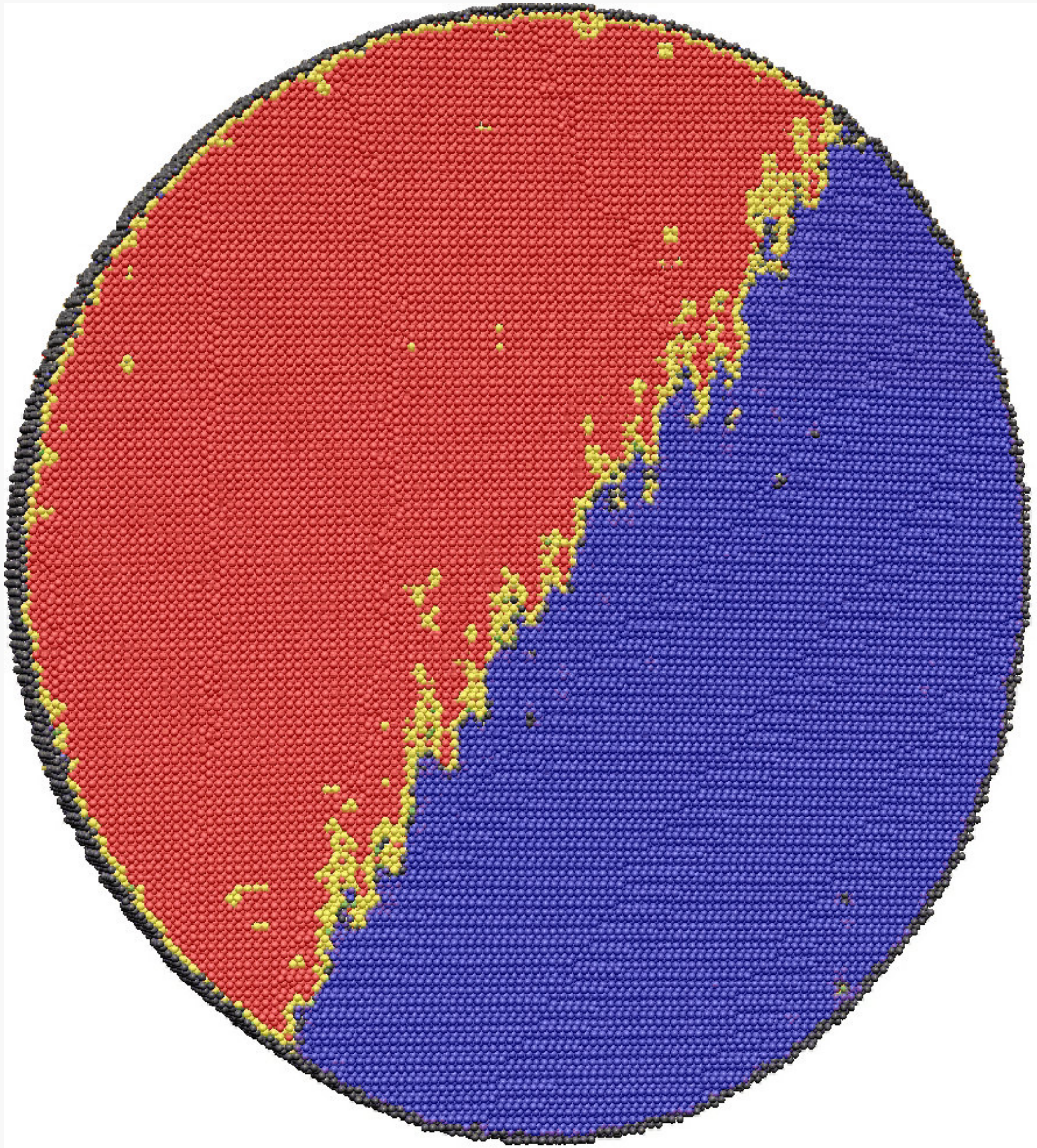

Radial Distribution Function

$$g(r) = \frac{V}{4\pi r^2 N^2} \left\langle \sum_i \sum_{j \neq i} \delta(r - r_{ij}) \right\rangle$$

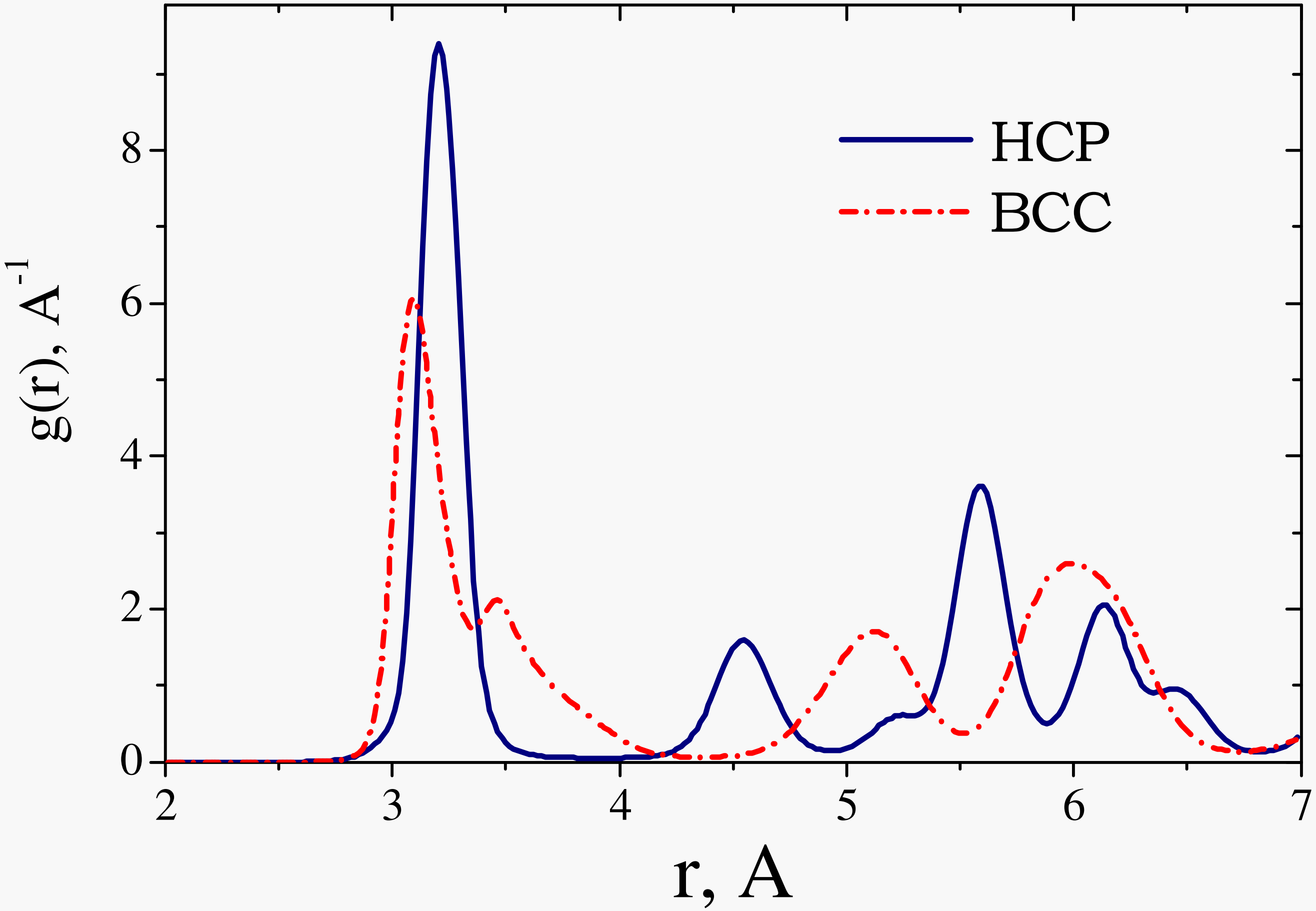

Local Order Characterization

1-st step: Voronoy tessellation

S. Nosé and F. Yonezawa, J. Chem. Phys. 84 (1979) 1803

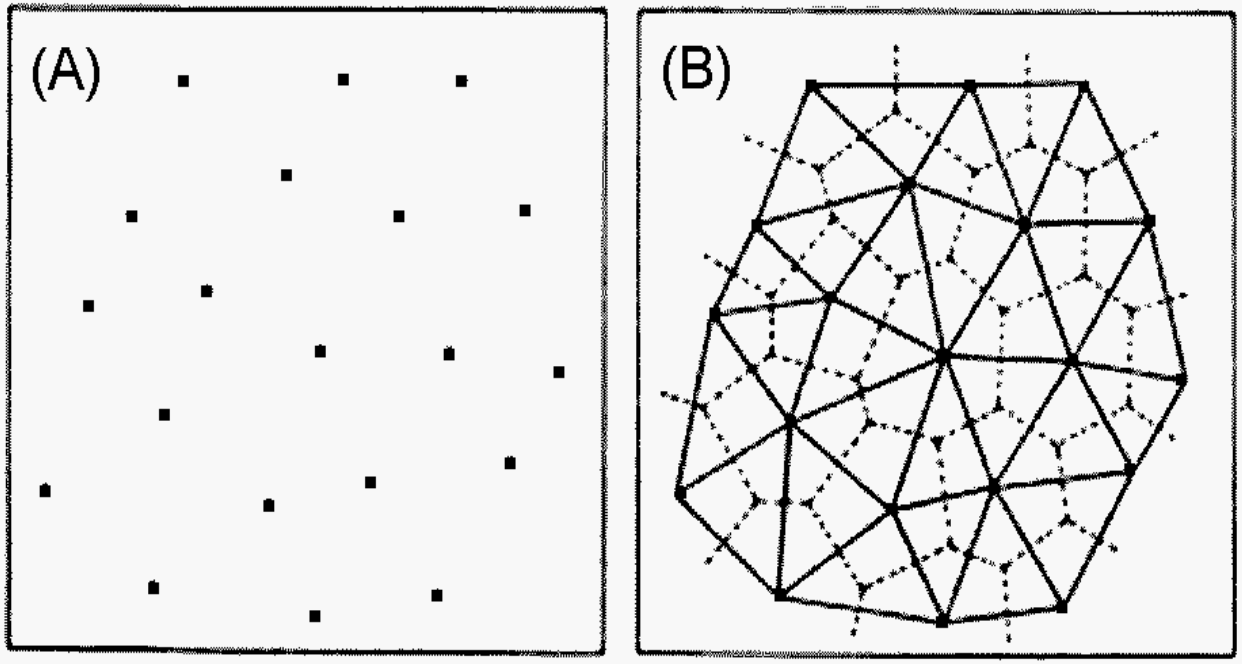

Definition of neighbors: *Voronoy polyhedra share a common face*

Local Order Characterization

2-nd step: Common Neighbors Analysis (CNA):

H. Jonsson, H. C. Andersen, *Phys. Rev. Lett. 60, (1988) 2295*

Bond index *lijk* :

i is the number of CNs.

j is the number of common bonds between the CNs.

k is the longest continuous chain formed by bonds between CNs.

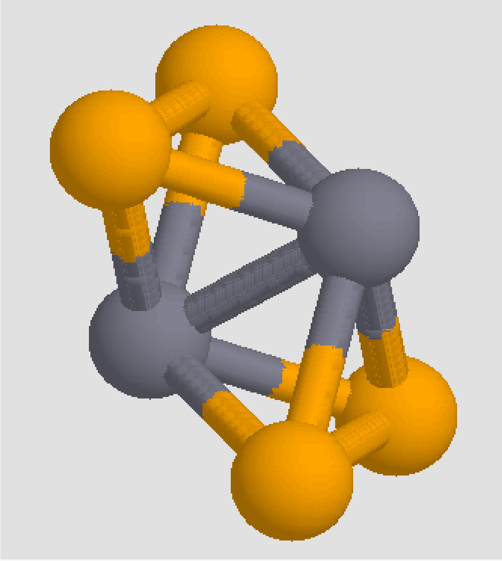

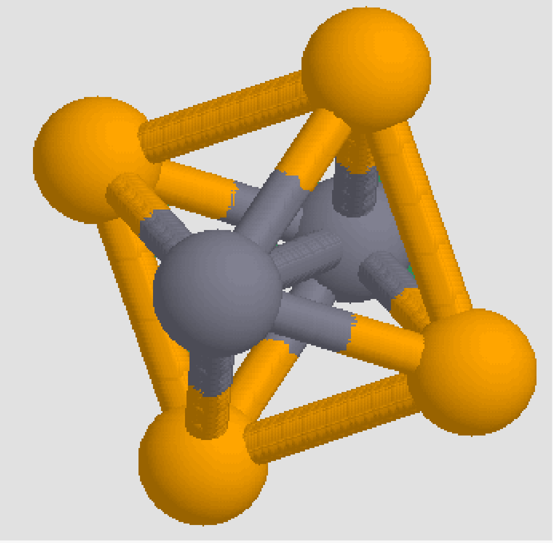

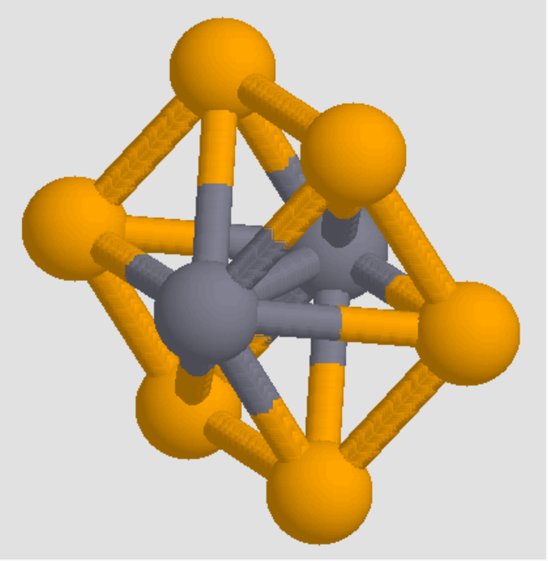

FCC = 12 x *1421*　　BCC = 8 x *1444* + 6 x *1666*

Structure of martensite state after transformation (PBC)

T = 1000K
N = 43904

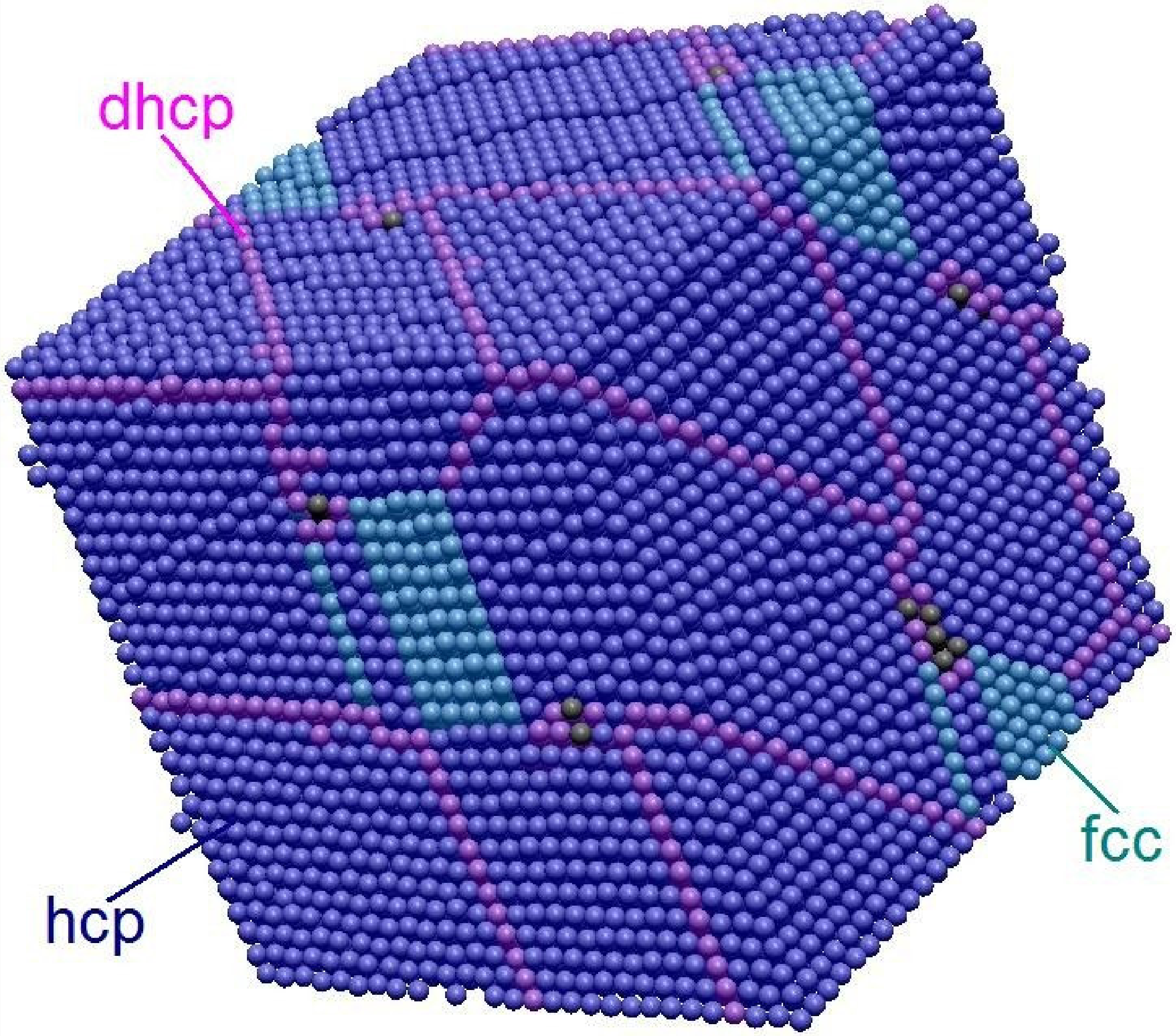

Perfect HCP
Perfect FCC
Distorted FCC + HCP
Perfect BCC
Distorted BCC
Perf. & Dist. ICO
Unclassified

Heterogeneous transformation $\beta \to \alpha$

T = 520K
N = 204300

Perfect HCP
Perfect FCC
Distorted FCC + HCP
Perfect BCC
Distorted BCC
Perf. & Dist. ICO
Unclassified

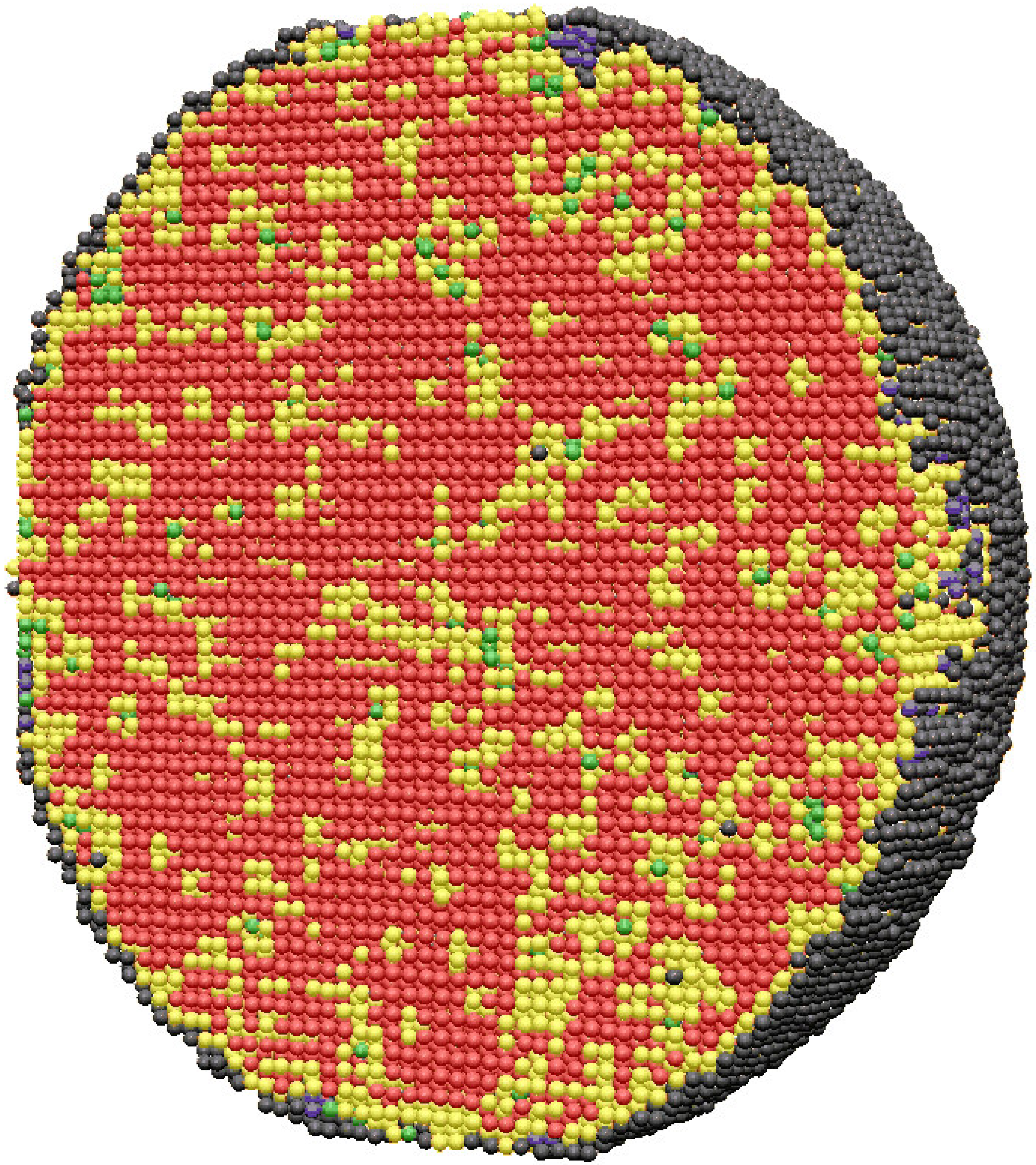

Reverse transformation α→β

T = 1560K
N = 204300

Perfect HCP
Perfect FCC
Distorted FCC + HCP
Perfect BCC
Distorted BCC
Perf. & Dist. ICO
Unclassified

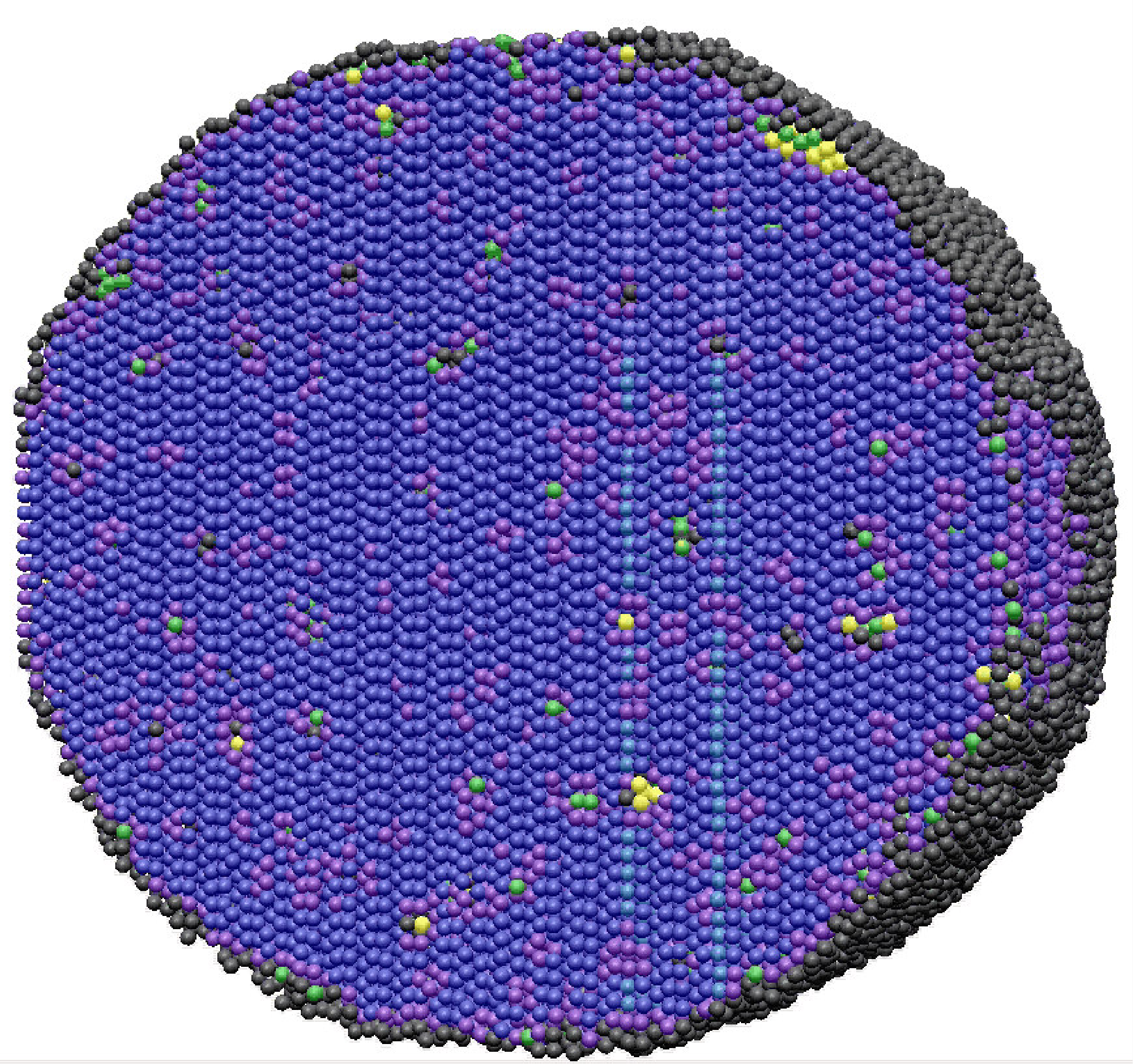

Initial and Final States at Transformation β→α

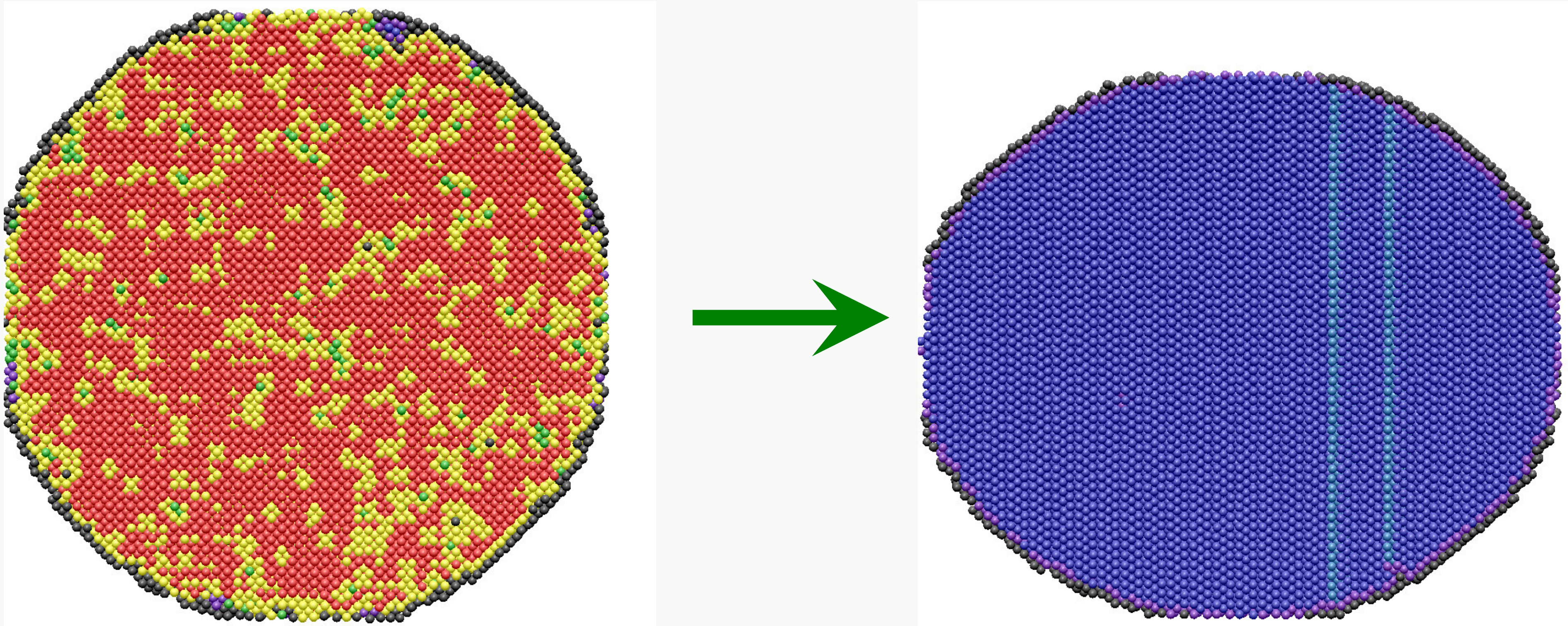

Initial and Final States at Transformation $\alpha \rightarrow \beta$

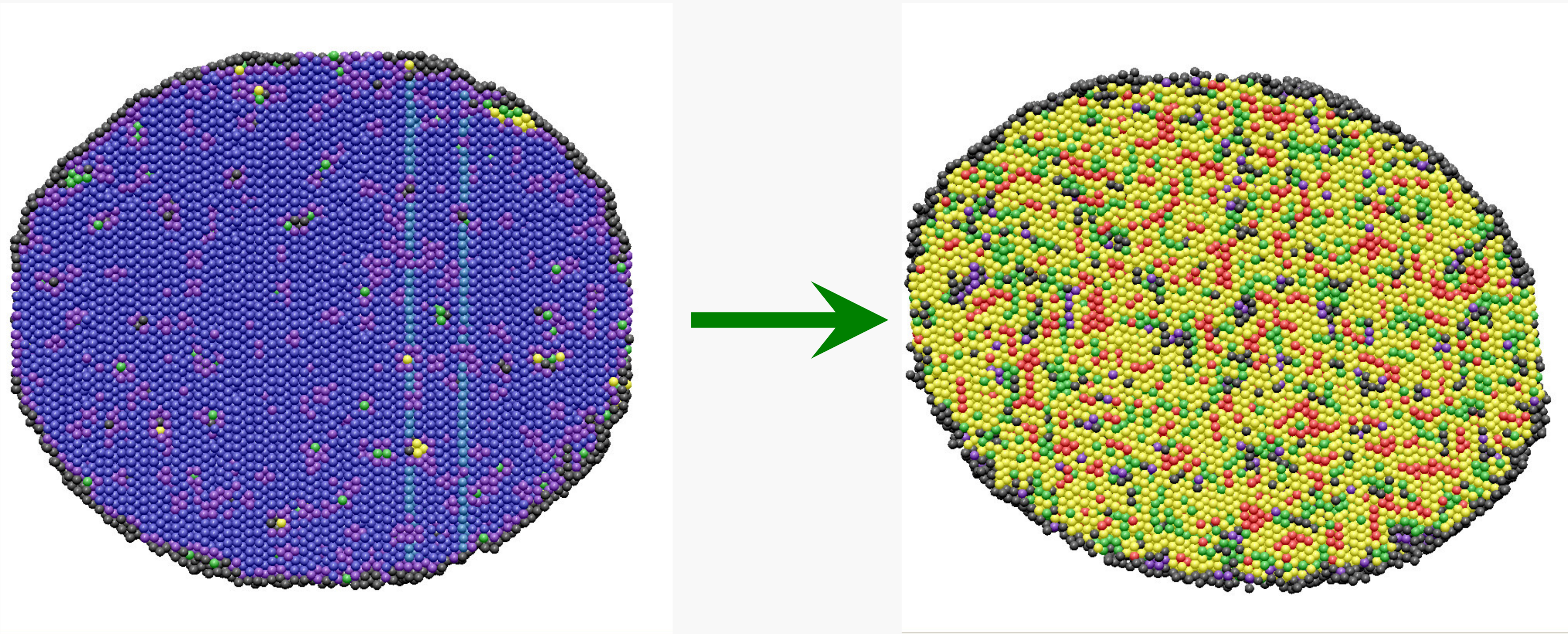

$\beta \rightarrow \alpha$ heterogeneous MT in polycrystalline Zr

N = 2 050 000

T = 800 K

Perfect FCC + HCP
Distorted FCC + HCP
Perfect BCC
Distorted BCC
Perf. & Dist. ICO
Unclassified

β→α heterogeneous MT in polycrystalline Zr

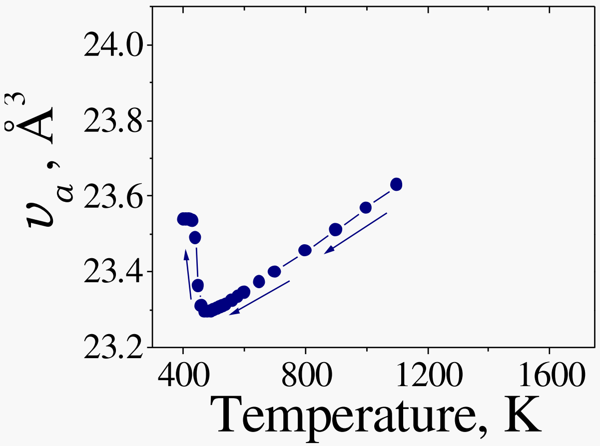

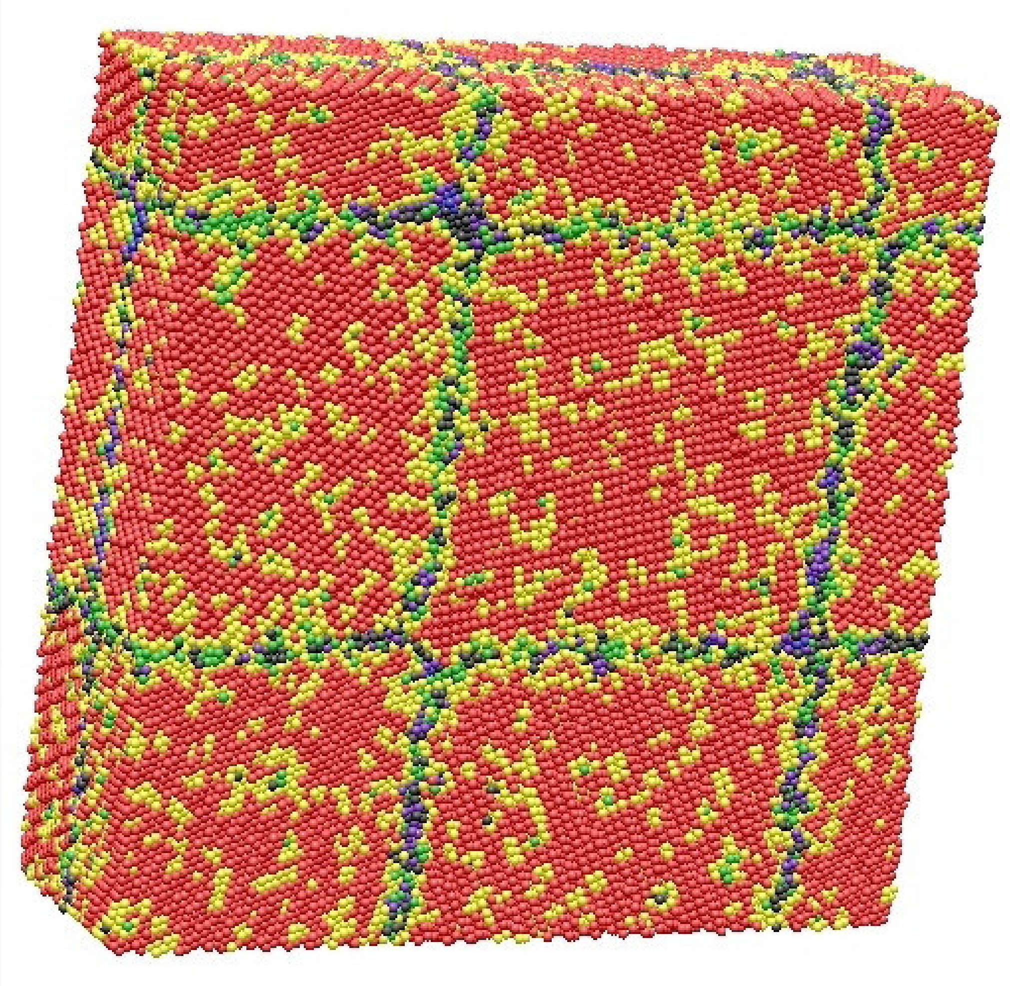

Perfect FCC + HCP
Distorted FCC + HCP
Perfect BCC
Distorted BCC
Perf. & Dist. ICO
Unclassified

N = 1 055 276

β→α heterogeneous MT in polycrystalline Zr

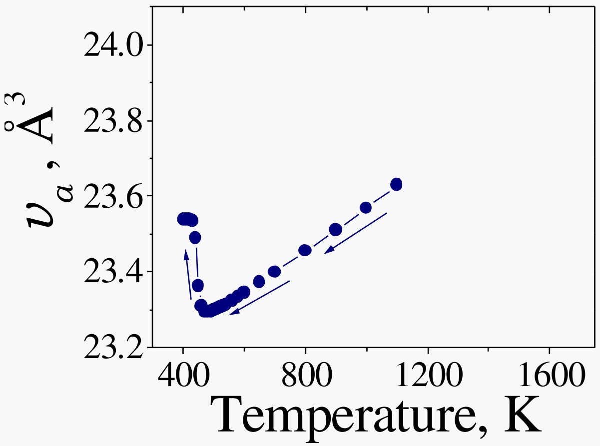

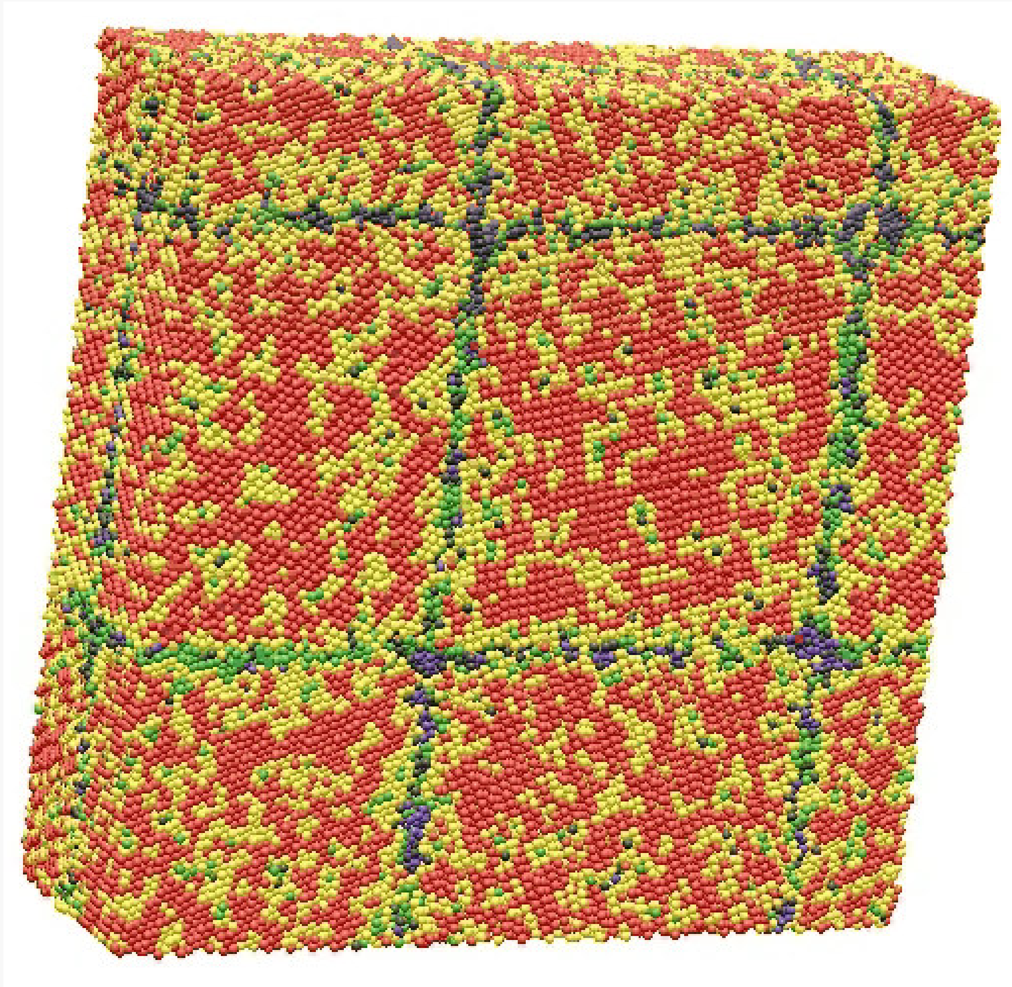

Perfect FCC + HCP
Distorted FCC + HCP
Perfect BCC
Distorted BCC
Perf. & Dist. ICO
Unclassified

N = 1 055 276

$\alpha \rightarrow \beta$ heterogeneous MT in polycrystalline Zr

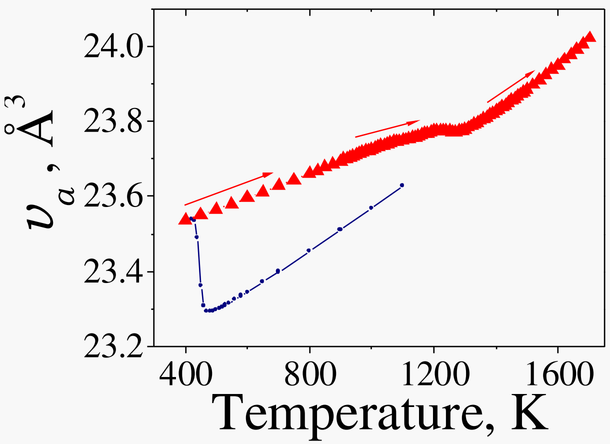

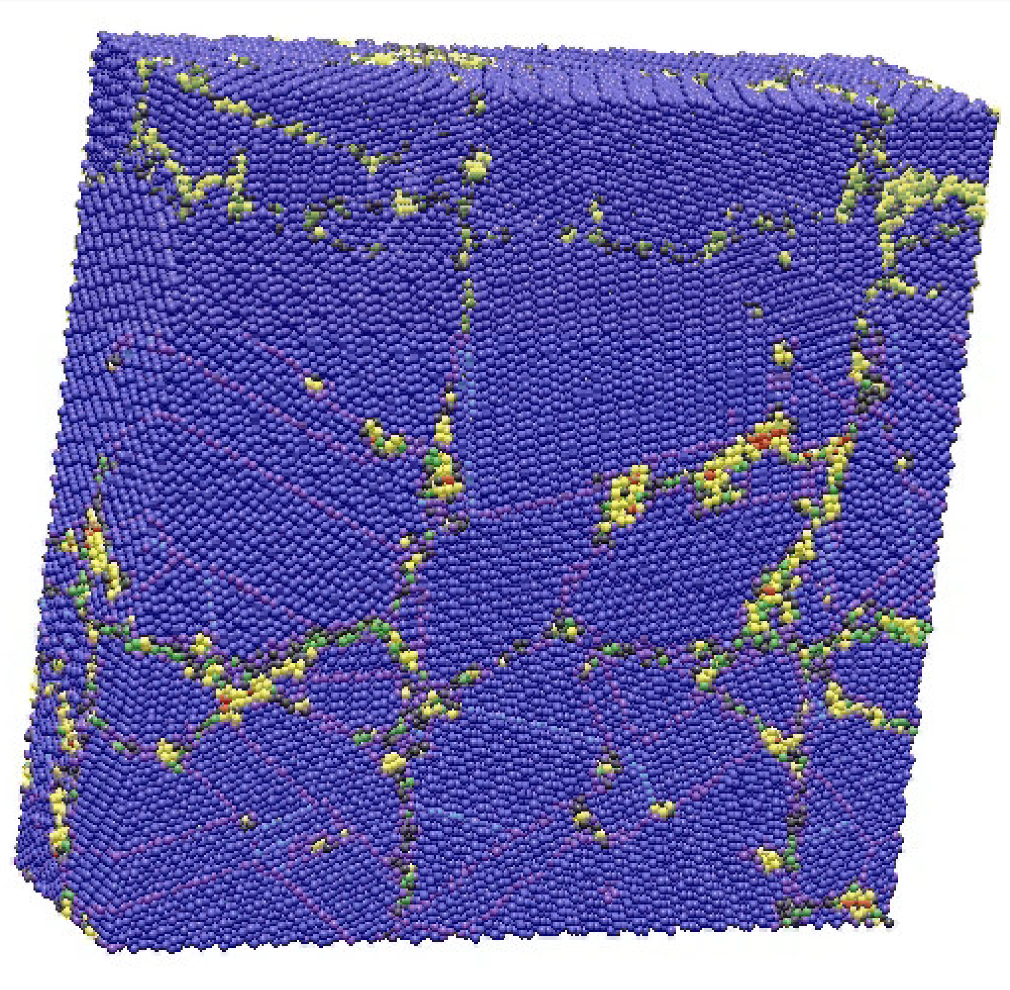

Perfect FCC + HCP
Distorted FCC + HCP
Perfect BCC
Distorted BCC
Perf. & Dist. ICO
Unclassified

N = 1 055 276

2-nd cycle of β→α heterogeneous MT in Zr

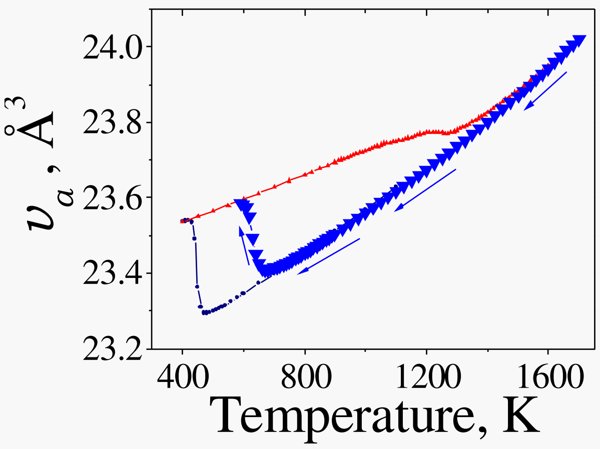

Perfect FCC + HCP
Distorted FCC + HCP
Perfect BCC
Distorted BCC
Perf. & Dist. ICO
Unclassified

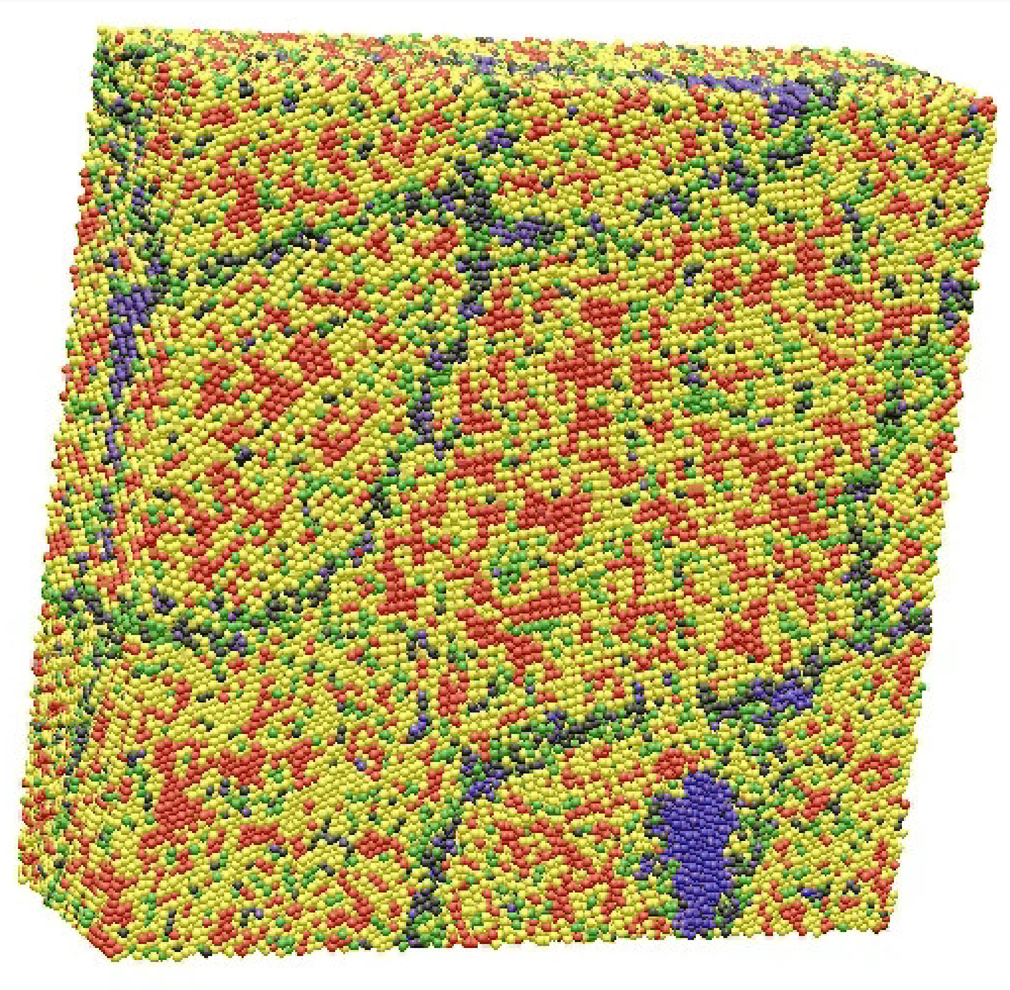

N = 1 055 276

Primary damages in displacement cascades

$N = 10^5 - 2 \cdot 10^6$

PKA energies: 0.01 – 20 keV

Temperatures: 300, 600, 900 K

Total cascades: > 600

$E_d \sim 24 - 20$ eV (T = 300 – 900 K)

MD time step *vs* fastest atom energy

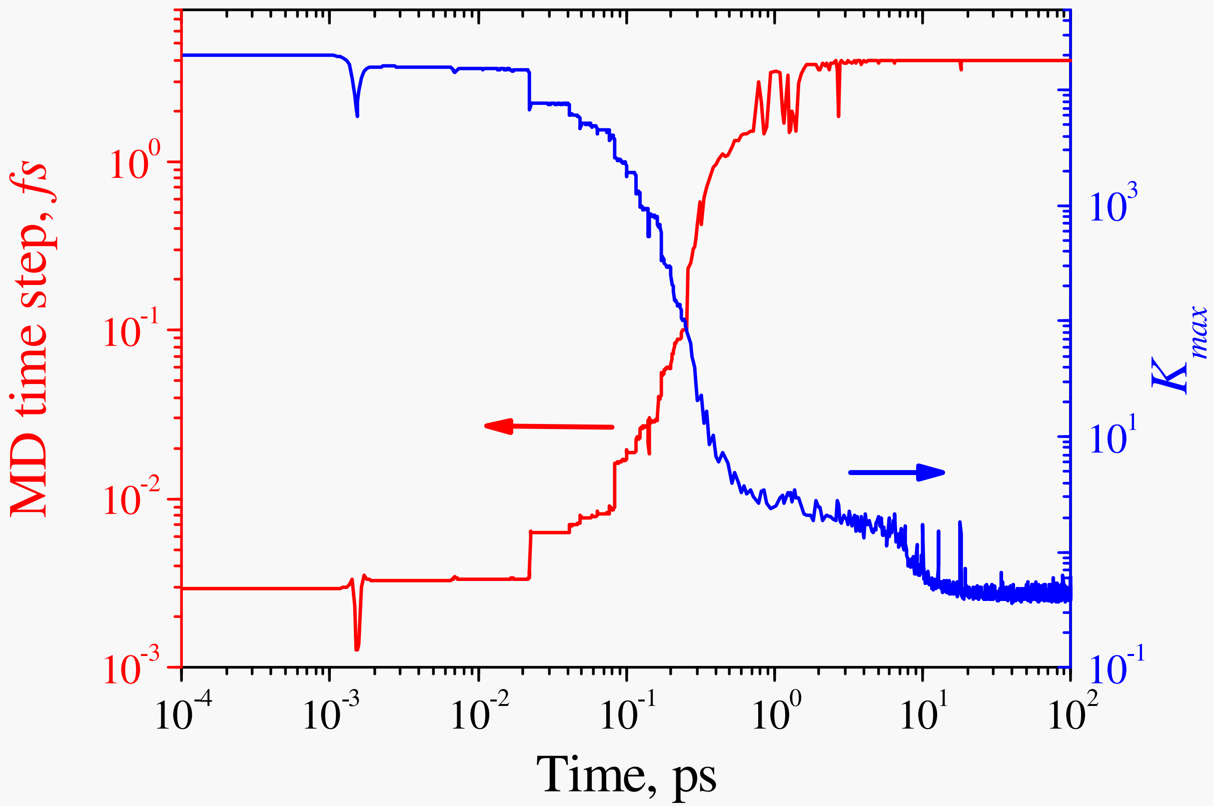

Point defect distribution, E_{PKA} = 20 keV, T = 300 K

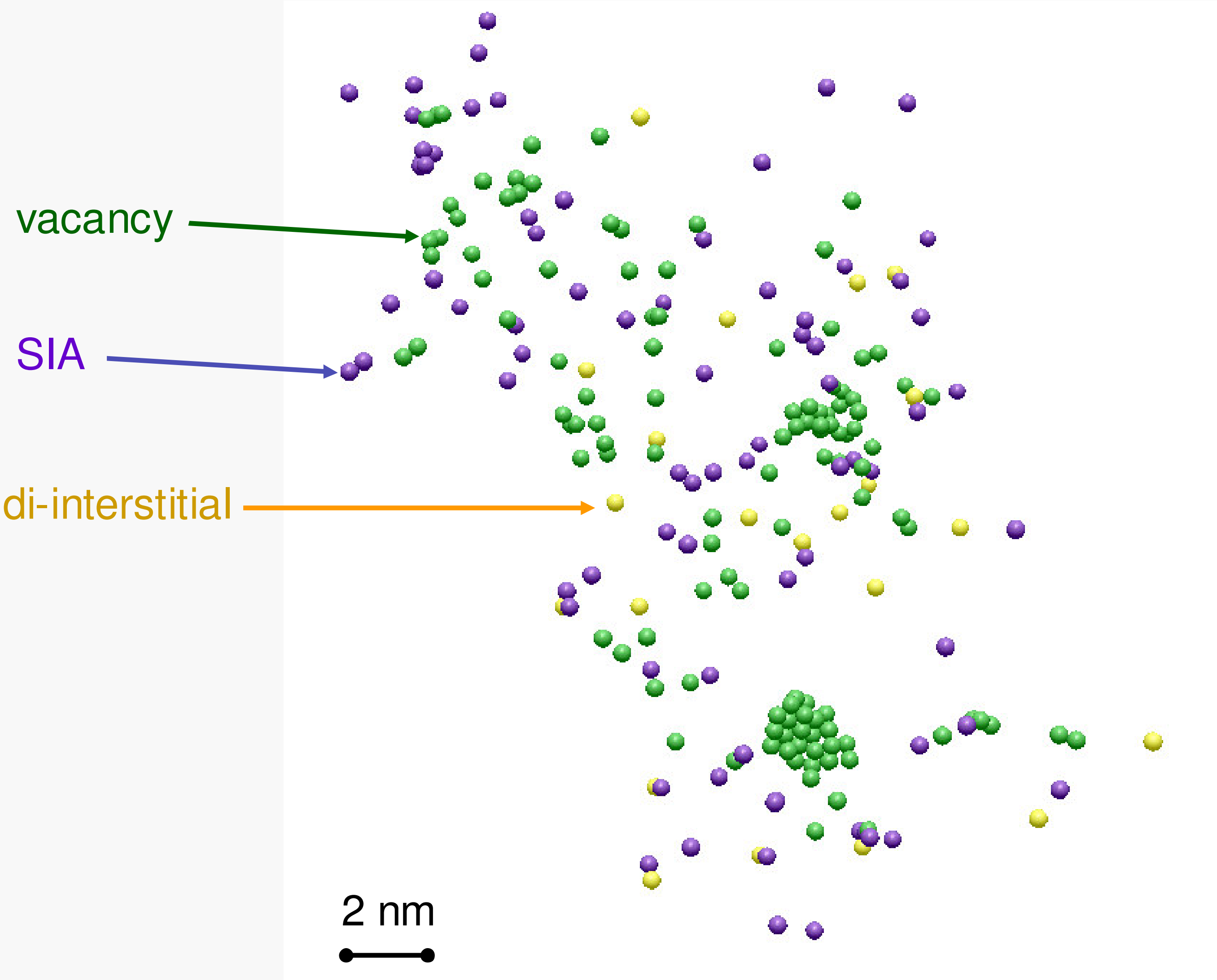

Defect production in Zr (MA potential) at T = 300K

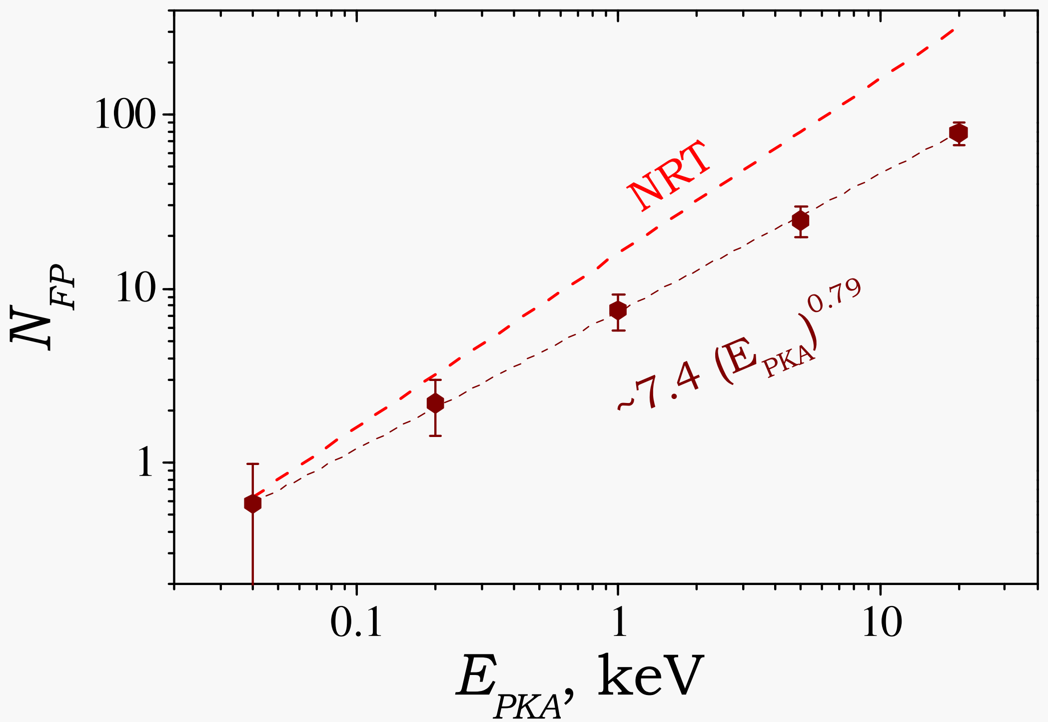

The standard Norgett-Robinson-Torrens (NRT) theory:

$$N_{NRT} = 0.8\, E_D / 2E_d$$

For simulated Zr (MA) we estimate threshold energy E_d = ***25*** *eV*

Defect production in Zr (MA potential) at T = 900K

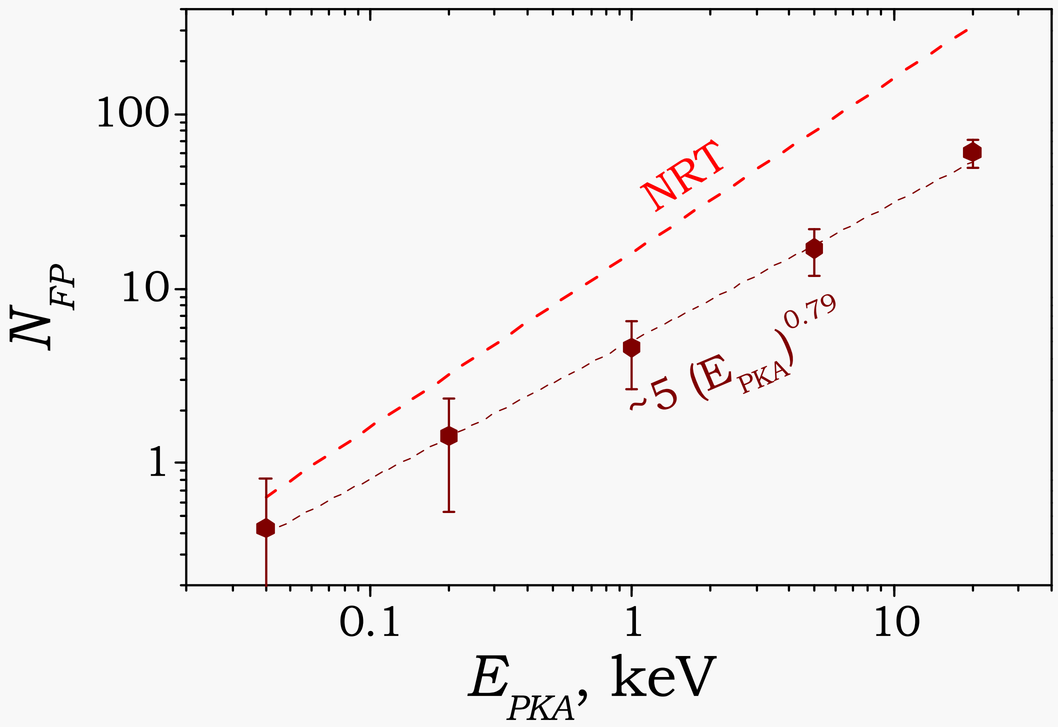

The number of the survived point defects decreases when the temperature rises.

Survived point defects fraction

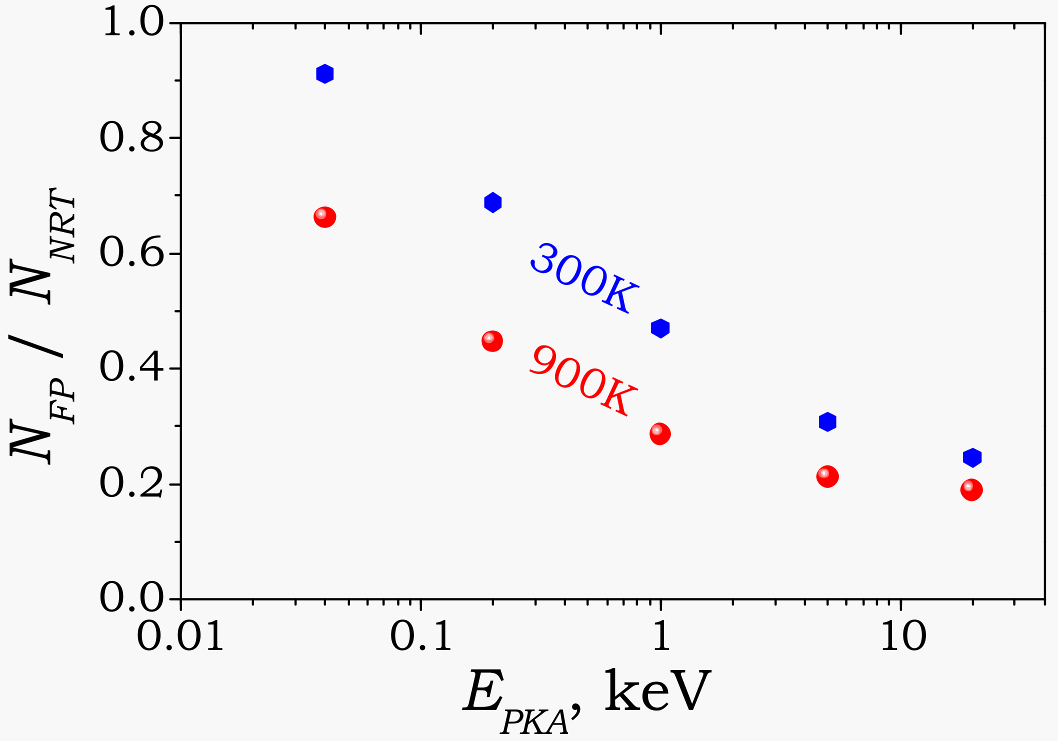

Damage production efficiency is degraded with increase cascade energy

Effect of cascade defects annealing at high temperature

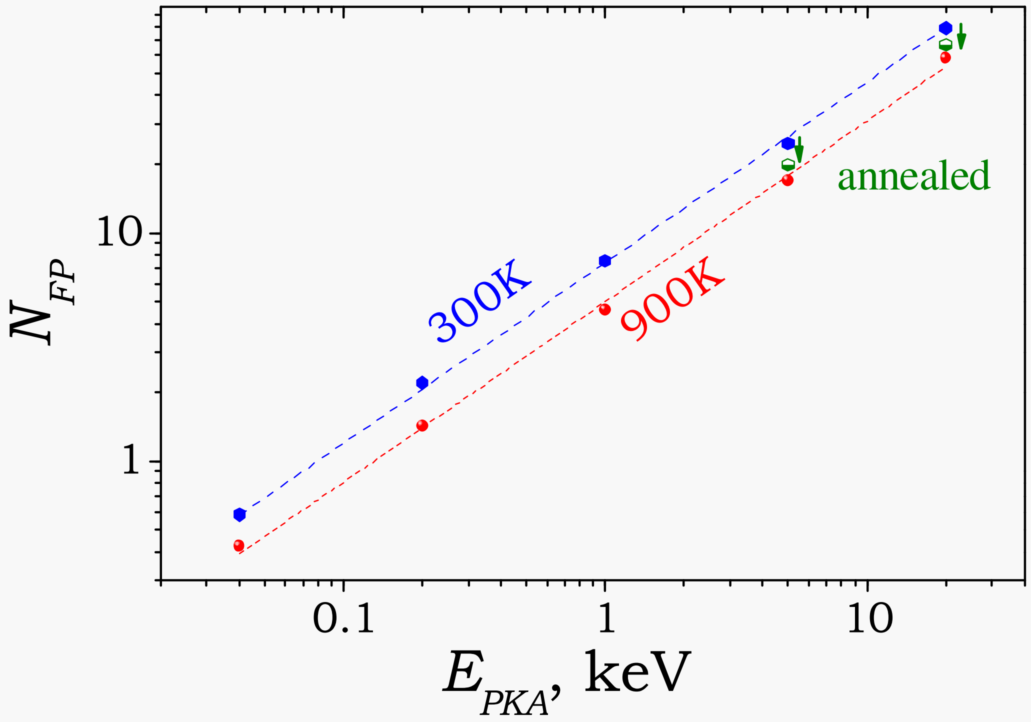

Annealing of low temperature cascade defects smoothes over the temperature effect

Defect production in Zr (AWB potential) at T = 300K

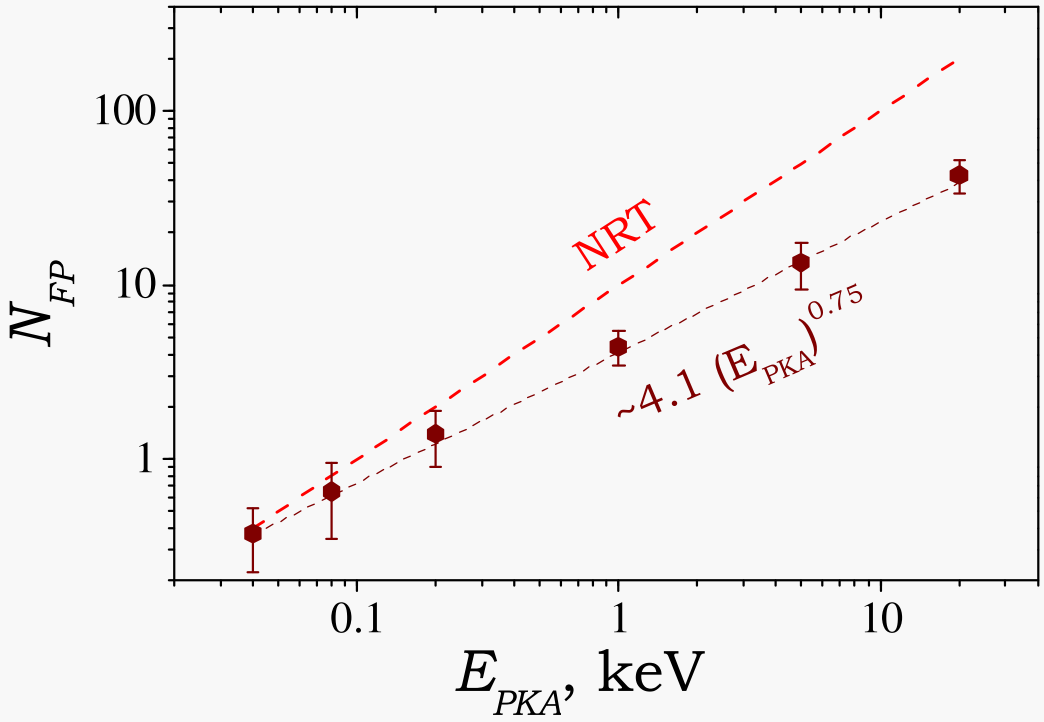

The standard Norgett-Robinson-Torrens (NRT) theory:

$$N_{NRT} = 0.8\, E_D / 2E_d$$

For simulated Zr (MA) we estimate threshold energy E_d = ***40*** *eV*

Defect production in Zr (AWB potential) at T = 900K

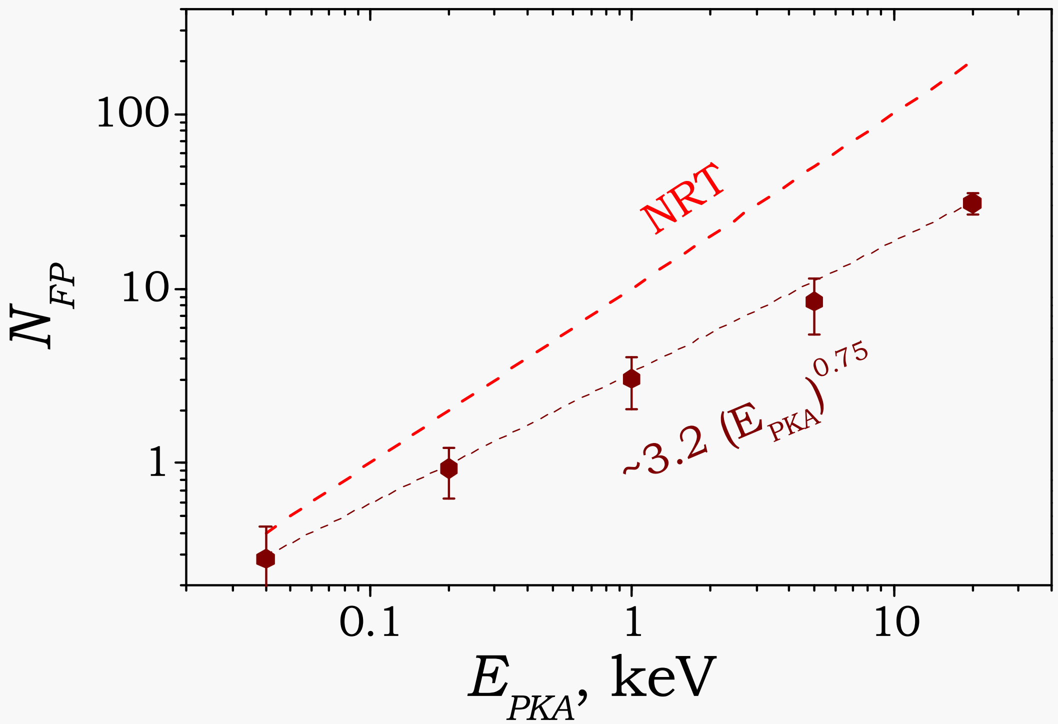

The number of the survived point defects decreases when the temperature rises.

Survived point defects fraction (AWB potential)

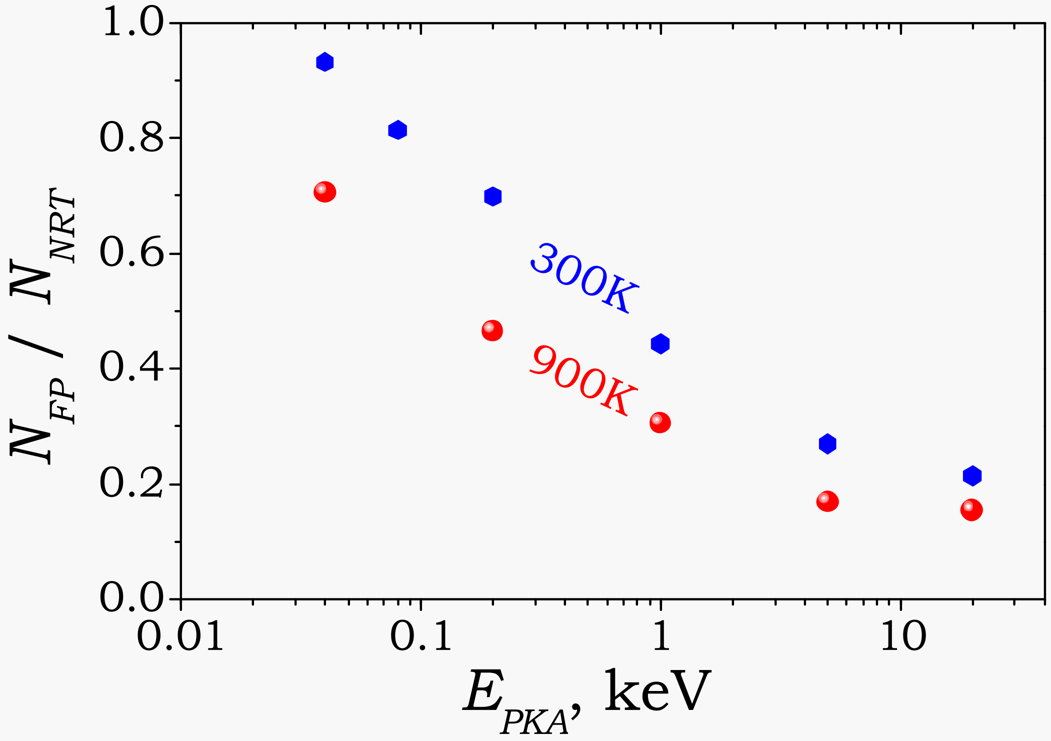

Damage production efficiency is degraded with increase of cascade energy

Distribution of cluster sizes (MA potential)

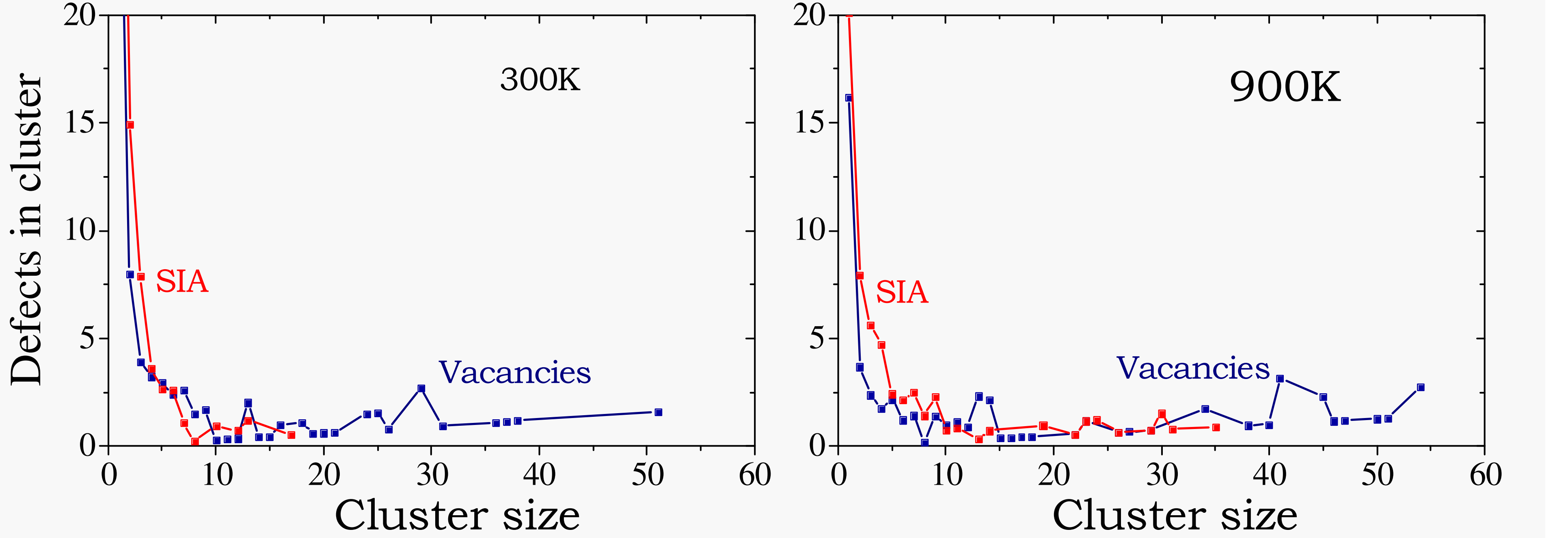

Vacancy clusters have broader distribution than SIA ones

Distribution of cluster sizes (AWB potential)

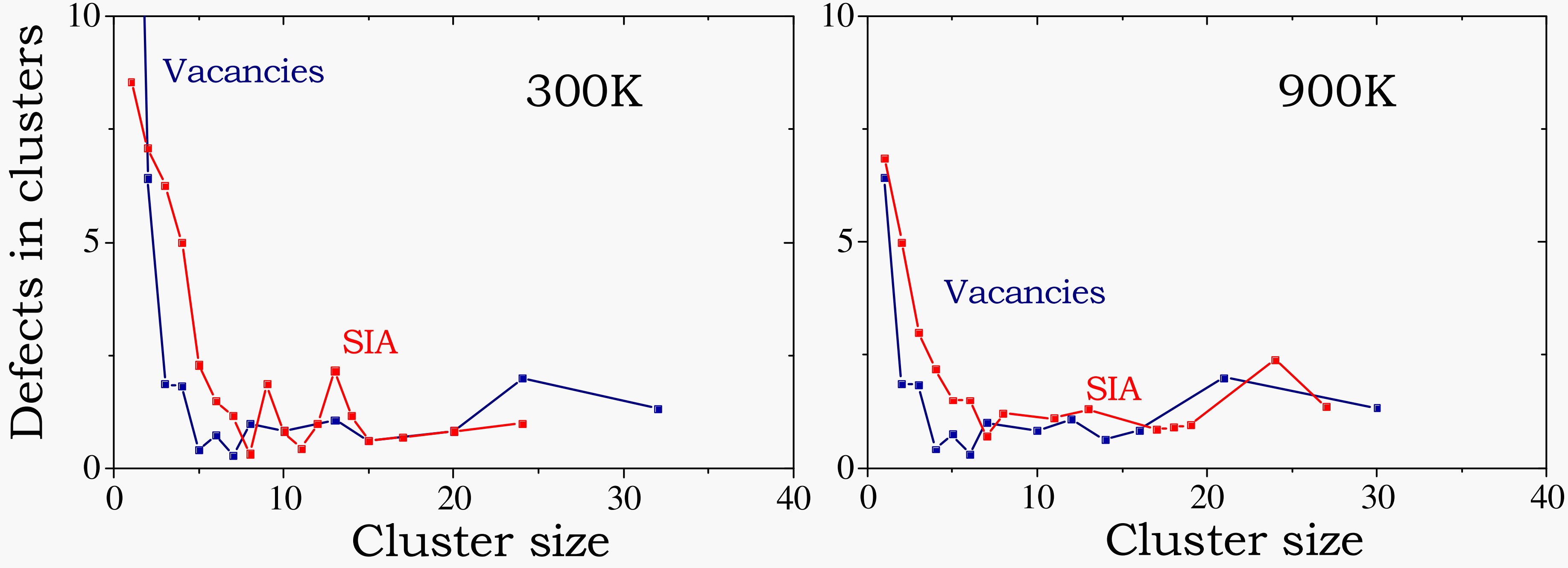

Vacancy and SIA clusters have similar distributions

Fraction of defects in clusters of size 2 and more (MA)

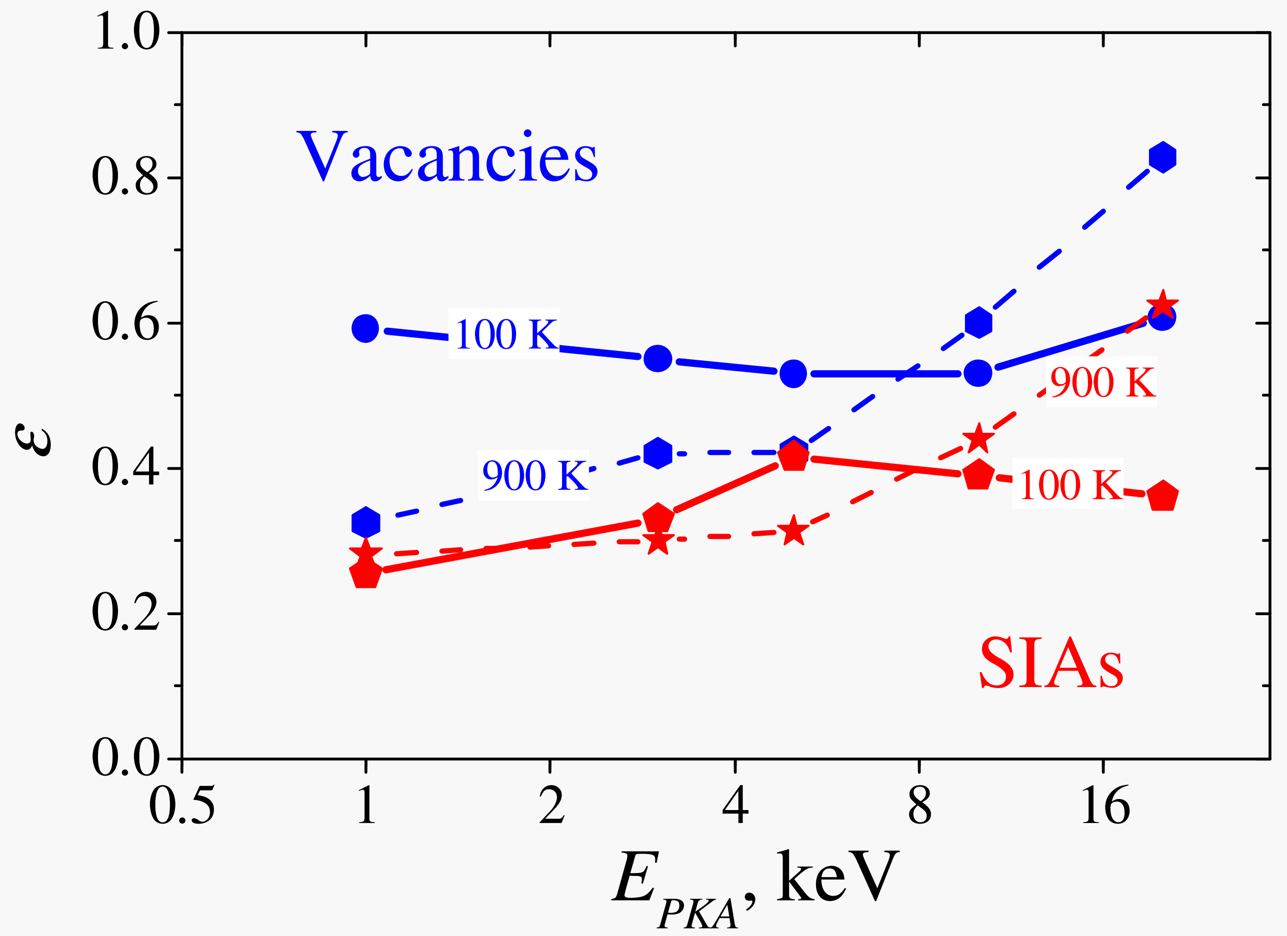

Conclusions

- A wide hysteresis is observed during reversible temperature-controlled MTs at MD simulation of model Zr. It is suggested that phase transformation kinetics is limited by nucleation processes in accordance with experiments
- Grain boundary affects the behavior of martensitic transformation. The hysteresis width becomes narrower indicating heterogeneous nucleation of new phase on the GB
- Local structure order parameter was implemented in the analysis of the displacive phase transformation kinetics
- Simulation of primary damage creation demonstrate increasing clusterization of point defects with PKA energy